International Journal of Multiphase Flow 193 (2025) 105355

Contents lists available at ScienceDirect

International Journal of Multiphase Flow

journal homepage: www.elsevier.com/locate/ijmulflow

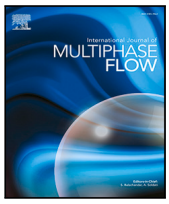

Research paper

Characterization of the critical lift-off of a single flat-plate microchip particle in straight rectangular microchannel flows

Raymond Yeung [a], Cynthia Sainz [b], Jason Mandala [c], Philip Brisk [d], William H. Grover [a], Victor G.J. Rodgers [a,*]

[a] Department of Bioengineering, University of California, Riverside, 92521, CA, USA
[b] Department of Evolution, Ecology, and Organismal Biology, University of California, Riverside, 92521, CA, USA
[c] Department of Electrical and Computer Engineering, University of California, Riverside, 92521, CA, USA
[d] Department of Computer Science and Engineering, University of California, Riverside, 92521, CA, USA

ARTICLE INFO

Keywords:
Lift-off
Critical
Pickup
Microfluidic
Particle
Non-spherical

ABSTRACT

Hydrodynamic sorting of microchip particles in microchannels is essential in microfluidic systems used for applications requiring particle-based multiplexing. Understanding the forces acting on the particle, as well as the dependencies of the forces on channel and fluid flow parameters, allows for prediction of the flow conditions needed to initiate particle movement, or lift-off. This study presents the experimental characterization of the lift-off of a single, flat-plate, non-neutrally buoyant microchip particle initially sedimented near the inlet of straight, rectangular microfluidic channels of different channel sizes and solvents at moderate Archimedes number of 191 to 2820. The critical shear Reynolds number, corresponding to the minimum required for lift-off, was found to increase with larger Archimedes number and the relationship was found to exhibit particle-channel size dependency. The observed critical lift-off for the flat-plate particle was lower than that predicted using a previous generalized lift-off model based on modified particle Reynolds and Archimedes numbers which may be explained by entrance effects and fluid film lubrication pressure under the particle. Numerical evaluations of the hydrodynamic forces acting on the particle revealed that electrostatic forces are significant. A remodified Archimedes number, based on the channel width, particle diameter, and solvent relative permittivity, is introduced as a correction to the generalized lift-off model to account for hydrodynamics and electrostatics affecting the lift-off of a flat-plate particle. This model is in good agreement with the generalized particle lift-off model and allows for prediction of flat-plate particle lift-off in microfluidic channels for a moderate range of Archimedes numbers.

1. Introduction

Lift-off, the initiation of motion and suspension of sedimented solid particles through hydrodynamic interactions from the surrounding fluid, is a key process for the transport of non-neutrally buoyant particles flowing in microchannels. Microfluidics has emerged as a preferred method for particle manipulation due to the continued advancements in microchannel fabrication and understanding of particulate microchannel flow dynamics in microchannels. Among the particle manipulation techniques used in microfluidic systems, such as acoustic, electrophoretic, and magnetic methods, hydrodynamics is widely used on its own due to the advantage of offering passive lateral and axial positioning of particles simply from controlling the operating fluid flow and channel dimensions (Amini et al., 2014). The optimal design and operation of microfluidics used for hydrodynamic particle manipulation and sorting depends upon the understanding of the channel and fluid parameters affecting lift-off, and the prediction of the minimum operating flow conditions necessary for particle entrainment.

There has been increasing interest in incorporating silicon-based, non-neutrally buoyant microchip particles into microfluidic systems for a variety of applications involving particle manipulation. Flat-plate, silicon microchips, which may be fabricated with ease and at scale from patterning and dicing of silicon wafers, have emerged as key particles to transport in microfluidic systems for screening (Hoffmann et al., 2007a,b) and combinatorial synthesis (Vastl et al., 2017; Xiao et al., 2000). For applications requiring microparticle encoding for multiplexed detections and reactions, microchips offer increased reliability of patterning and significantly greater number of unique encoding combinations over other microparticles (Li et al., 2010). Moreover, the

* Corresponding author.
E-mail address: victor.rodgers@ucr.edu (V.G.J. Rodgers).

https://doi.org/10.1016/j.ijmultiphaseflow.2025.105355
Received 12 December 2024; Received in revised form 3 June 2025; Accepted 4 July 2025
Available online 25 July 2025

surface of silicon microchips may be functionalized for tailored applications (Birtwell and Morgan, 2009; Li et al., 2010, 2015). Flat-plate, silicon microparticles used in microfluidics have included microbarcodes that are optically encoded (Cunin et al., 2002; Eun Chung et al., 2009; Hoffmann et al., 2006, 2007b; Jensen-McMullin et al., 2008) and also microtransponders that store codes in memory and transmit the codes using radio frequency (Mandecki et al., 2006).

However, there is a lack in understanding of the particulate flow behavior, including lift-off, of these non-spherical, non-neutrally buoyant microparticles in microfluidic channels. Therefore, an investigation of the channel configurations and fluid parameters affecting lift-off of flat-plate, non-neutrally buoyant microparticles in microchannels is needed to develop a model to predict the minimum operating flow conditions for hydrodynamic-induced movement of this subset of particles in different microfluidic particulate flow systems.

Initiation of particle movement through pneumatic conveying (PC) and hydraulic conveying (HC) has been practiced for centuries and significant work has been performed in the last several decades to develop methodologies to predict the flow conditions necessary for lift-off of single and multiple particles from a sedimented particulate layer. Many terms are used in literature to refer to the threshold, or minimum, fluid flow conditions for suspension of sedimented particles during horizontal conveying: pickup (gas in pipes), wind (gas in large tunnels), critical (liquid in pipes and channels), lift-off (liquid in Poiseuille flow), and detachment (liquid in cylindrical microchannel; or air through a plug). For clarity, these terms for suspension differ from saltation. Suspension involves particles that are initially sedimented whereas for saltation, the particles are initially suspended.

Moreover, there are many different parameters used in empirical and theoretical models to describe the fluid flow for particle suspension. The threshold fluid velocity is typically expressed in terms of the average fluid velocity, $\langle U \rangle$, or maximum fluid velocity, $U_{\max}$. However, the shear velocity, $U_* = \sqrt{\tau/\rho_f}$, where τ is the shear stress at an arbitrary fluid layer and ρ_f is the fluid density, is also extensively used in theoretical models since the threshold shear velocity represents the fluid velocity profile around the particle and wall. Several dimensionless numbers have been developed to derive models for different conveying systems. The parameters affecting the vertical flow have been described using the Froude number (Fr), the square root of the ratio of the inertial force and the particle weight, and the Archimedes number (Ar), the square of the ratio of the gravitational force and viscous force. While Fr is found to be valid for PC systems (Cabrejos and Klinzing, 1992, 1994), it has been found to be invalid for HC systems. The Archimedes number, which captures the effect of buoyancy, has been demonstrated to be more appropriate for analysis of both PC (Kalman et al., 2005; Rabinovich and Kalman, 2007) and HC (Rabinovich and Kalman, 2007, 2008, 2009a,b) systems. The parameters affecting the horizontal flow, which is dominated by the inertial force and opposing viscous force, have been described using the Reynolds number (Re), particle Reynolds number ($\mathrm{Re_p}$), and shear Reynolds number ($\mathrm{Re_s}$), in relation to the channel, particle, and shear flow, respectively (Patankar et al., 2001; Kalman, 2022).

Extensive experimental and analytical work have been performed towards predicting the critical fluid flow conditions for suspension of particles in relatively large channels (25 to 150 mm in diameter) for horizontally-oriented HC processes. Kalman and Rabinovich gathered experimental data from various studies to develop a generalized empirical model to predict the threshold $\mathrm{Re_p}$ for particle suspension as a function of Ar (Kalman et al., 2005; Rabinovich and Kalman, 2007, 2008, 2009a,b). Critical suspension is dependent on many factors including the fluid density, number of particles (single or layer of particles), channel diameter or width, particle shape, and particle friction coefficient. Rabinovich and Kalman (2009a) compiled experimental data from studies on the incipient motion of a single particle in air (Halow, 1973; Cabrejos and Klinzing, 1992; Stevenson et al., 2002; Hubert and Kalman, 2004; Rabinovich and Kalman, 2009a) and water (Han and Hunt, 1995) in horizontal particulate flow systems. They proposed a generalized power law relationship, which accounted for the effect of the channel diameter and particle friction coefficient, to predict the critical $\mathrm{Re_p}$ for lift-off of a single particle as a function of Ar. The collection of studies from the authors provide the most comprehensive set of particle lift-off analyses to date. However, since the particulate flow experiments used relatively large channels, with ratios of particle diameter to channel diameter ranging from 0.009 to 0.049, the effect of the channel walls on the particle lift-off was not studied. Also, while Rabinovich and Kalman (2009a) conducted experiments using spherical and non-spherical particles to develop the empirical generalized lift-off model, the particle shapes were not tightly controlled nor described. Electrostatic effects were also precluded from their studies.

Only a few studies have investigated the threshold flow conditions for particle lift-off in microchannels. Direct numerical simulation of a single circular particle in planar Poiseuille flow through a rectangular microchannel using an arbitrary Lagrangian-Eulerian (ALE) method indicated that the critical shear Reynolds number for particle lift-off decreases as the ratio of the channel height and the particle rotational diameter, $H/d_{\max}$, also referred to as the height domain size, increases (Patankar et al., 2001). The simulation data could be represented by power law equations for each $H/d_{\max}$. In a separate work, experimental studies of the lift-off of spherical particles in cylindrical microchannels showed that the detachment fluid velocity decreased as the ratio of the channel diameter and the particle rotational diameter, $D/d_{\max}$, increases (Shukla and Henthorn, 2009). Importantly, these previous works on lift-off in microchannels reveal that at the microfluidic level, where the particle-channel size ratio is relatively large, wall effects play a significant role in the critical lift-off. However, the studies consider only the 1-D channel geometry contribution to lift-off. Also, the studies ignore entrance and electrostatic effects. Moreover, the studies do not extend their lift-off analysis to oblate or flat particles.

In this study, we experimentally investigated the hydrodynamic lift-off of a single sedimented flat-plate, non-neutrally buoyant microchip particle in straight, horizontally-aligned, rectangular cross-section microchannels. Using different combinations of solvents (isopropyl alcohol, water, and methanol) and microchannels of different cross-sectional sizes, we examined the effects of the solvent properties and channel dimensions on the critical shear Reynolds number for lift-off. Through dimensional analysis and comparison of our data on critical lift-off of flat-plate particles to that of spherical particles from previous studies, we re-examined the use of the channel-particle size parameter, typically defined as $H/d_{\max}$, in expressing the dependency of the critical shear Reynolds number on the particle-channel size. We proposed and demonstrated that both the ratio of the channel area over the particle rotational diameter squared, $HW/d_{\max}^2$, also referred to as the area domain size, as well as the channel aspect ratio, $AR = H/W$, are needed for prediction of flat-plate particle lift-off in rectangular microchannels. While many previous lift-off studies place particles near the middle of the channel length to eliminate entrance and end effects in the analysis, practical particle sorting applications typically involve preloading particles towards a physical particle mesh or trap integrated into the microfluidic system. Moreover, electrostatics are often eliminated in experimental particulate flow characterizations. In consideration of pragmatic applications, we performed experimental particle lift-off studies with the microchip particle beginning at rest near a physical particle trap upstream of each rectangular microchannel. Towards assessing the effect of the trap and the positioning of the particle at the inlet on the observed particle lift-off, we performed computational fluid dynamics (CFD) simulations of a stationary particle at various locations along the channel length, and evaluated the hydrodynamic and electrostatic forces on the particle. In efforts to verify and improve empirical models for critical lift-off of particles in microfluidic channels, we mapped our single flat-plate particle lift-off

data to a previously developed generalized model for lift-off in horizontal particulate flow systems. We introduced a remodified Archimedes number, which accounts for the lift-off dependency on the channel geometry, particle-channel size, and electrostatic adhesion, to develop an empirical model for accurate prediction of lift-off of a flat-plate particle in a rectangular, microfluidic particulate flow systems.

2. Modeling approaches

2.1. Dimensionless numbers

For our analysis, we used the channel Reynolds number, particle Reynolds, and shear Reynolds number to capture parameters affecting horizontal fluid flow, and the Archimedes number to describe parameters affecting the vertical fluid flow. The dimensionless numbers for the analysis of lift-off in horizontal hydraulic conveying in microchannels include:

$$\mathrm{Re} = \frac{\rho_\mathrm{f}\langle U\rangle D_\mathrm{H}}{\mu} \quad \text{channel Reynolds number} \tag{1}$$

$$\mathrm{Re}_{\mathrm{p},d} = \left(\frac{d}{D_\mathrm{H}}\right)^2 \mathrm{Re} \quad \text{particle Reynolds number} \tag{2}$$

$$\mathrm{Re}_{\mathrm{s},d} = \frac{\rho_\mathrm{f}\langle\dot{\gamma}_\mathrm{w}\rangle d^2}{\mu} \quad \text{shear Reynolds number} \tag{3}$$

$$\mathrm{Ar}_d = \frac{\rho_\mathrm{f}(\rho_\mathrm{p}-\rho_\mathrm{f})g d^3}{\mu^2} \quad \text{Archimedes number} \tag{4}$$

where ρ_f is the fluid density, $\langle U\rangle$ is the average fluid velocity, D_H is the channel hydraulic diameter, μ is the fluid dynamic viscosity, d is the characteristic particle diameter, $\langle\dot{\gamma}_\mathrm{w}\rangle$ is the average shear rate at the bottom channel wall, ρ_p is the particle density, and g is the standard acceleration of gravity. It is noted that the critical velocity, used in the evaluation of Eqs. (1) and (3), is the superficial velocity, the flow velocity evaluated with only the fluid present. To compare our experimental lift-off data to that of other studies that use different definitions to describe the size of the non-spherical particle, we considered both commonly used definitions of d: the particle rotational diameter, d_max, and the equivalent volume spherical particle diameter, d_V. For our study of a square prism, flat-plate particle (consisting of a height of h, and a square base with an edge width of w), the rotational diameter is defined as $d_\mathrm{max} = w\sqrt{2}$ and the equivalent volume spherical particle diameter is defined as $d_\mathrm{V} = (6hw^2/\pi)^{1/3}$. It is acknowledged that for a non-spherical particle, its shape and orientation affects the forces acting on the particle and the resulting dynamics of the flowing particle. While orientation-dependent models have been developed to characterize particulate flow behaviors (Mandø and Rosendahl, 2010; Gallily and Cohen, 1979), simplified models based solely on particle descriptors, such as the characteristic particle diameter, have been shown to be effective in predicting particle flow dynamics including inertial focusing (Hur et al., 2011) and incipient motion of particles (Rabinovich and Kalman, 2009b,a).

2.2. Models of single particle lift-off in horizontal flow systems

Patankar et al. (2001) performed 2-D direct numerical simulations of the lift-off of a single spherical particle in planar Poiseuille flow. They observed that the critical shear Reynolds number, $\check{\mathrm{Re}}_{\mathrm{s},d_\mathrm{max}}$, for lift-off at a given Archimedes number, $\mathrm{Ar}_{d_\mathrm{max}}$, decreases as H/d_max increases; an asymptotic value for $\check{\mathrm{Re}}_{\mathrm{s},d_\mathrm{max}}$ is reached above a certain H/d_max. An empirical relationship between $\check{\mathrm{Re}}_{\mathrm{s},d_\mathrm{max}}$ and $\mathrm{Ar}_{d_\mathrm{max}}$ at a specified H/d_max may be described using a power law equation:

$$\mathrm{Ar}_{d_\mathrm{max}} = a\left(\check{\mathrm{Re}}_{\mathrm{s},d_\mathrm{max}}\right)^b \tag{5}$$

where a and b are fitted parameters for each H/d_max.

In related work, Kalman and Rabinovich conducted particle lift-off experiments, using a variety of both spherical and non-spherical particles, and compiled experimental data from other works to generate a generalized curve for threshold suspension in different particulate flow systems (Kalman et al., 2005; Rabinovich and Kalman, 2007, 2008, 2009a). From the hundreds of experiments collected, a power law relationship between the $\check{\mathrm{Re}}_{\mathrm{p},d_\mathrm{V}}$ and $\mathrm{Ar}_{d_\mathrm{V}}$ effectively described the data with over 90% of the experiments within ± 30% error:

$$\frac{\check{\mathrm{Re}}_{\mathrm{p},d_\mathrm{V}}}{r} = c(\mathrm{Ar}_{d_\mathrm{V}}k)^m \tag{6}$$

where r is a parameter adjusting $\check{\mathrm{Re}}_{\mathrm{p},d_\mathrm{V}}$ to account for different channel sizes used in the experiments, c is an empirical parameter, k is a parameter adjusting $\mathrm{Ar}_{d_\mathrm{V}}$ by an additional effect based on particle properties (particle sphericity, ϕ, or static friction coefficient, μ_sf), and m is an empirical power term. The parameters used in Eq. (6) are dependent on various factors, including, but not limited to, the type of threshold process (suspension or saltation), number of particles (single particle or a layer of particles), medium of fluid (gas or liquid), defining the particulate flow conditions of the studied system.

For the remaining discussion, the dimensionless parameters presented will be those corresponding to that from an empirical expression for the critical lift-off of a single particle from a rectangular channel in liquid flow adapted from Rabinovich and Kalman (2009a). A modified critical particle Reynolds number, $\check{\mathrm{Re}}^*_{\mathrm{p},d_\mathrm{V}} = \check{\mathrm{Re}}_{\mathrm{p},d_\mathrm{V}}/r$, is defined such that for rectangular channels, each with a hydraulic diameter $D_\mathrm{H} = (2HW/(H+W))$, the measured critical average velocities may be converted to that for a reference 50 mm diameter (D_{50}) cylindrical pipe using an exponentially bounded function:

$$\check{\mathrm{Re}}^*_{\mathrm{p},d_\mathrm{V}} = \frac{\check{\mathrm{Re}}_{\mathrm{p},d_\mathrm{V}}}{(1.25 - 0.5\exp(-(D_\mathrm{H}/D_{50})/1.5))} \tag{7}$$

It is noted that D_H in Eq. (7) has replaced D, defined as the diameter of a cylindrical pipe or as the channel width W for experiments involving a square duct, from the original expression for incipient motion of a single particle in liquid channels formulated by Rabinovich and Kalman (2009a).

To account for the effect of friction between the particle and channel wall, Rabinovich and Kalman (2009a) proposed a modified Archimedes number, $\mathrm{Ar}^*_{d_\mathrm{V}} = \mathrm{Ar}_{d_\mathrm{V}}k$, also defined as:

$$\mathrm{Ar}^*_{d_\mathrm{V}} = \mathrm{Ar}_{d_\mathrm{V}}\mu_\mathrm{sf} \tag{8}$$

where μ_sf is the static particle–wall friction coefficient.

Based on experiments of individual large particles ($d > 0.4$ mm) in horizontal conveying systems, Rabinovich and Kalman (2009a) determined the following relationship for the critical lift-off of a single particle in a channel:

$$\check{\mathrm{Re}}^*_{\mathrm{p},d_\mathrm{V}} = 2.7\mathrm{Ar}^{*\,3/7}_{d_\mathrm{V}} \qquad 8000 < \mathrm{Ar}^*_{d_\mathrm{V}} < 8.7\times10^6 \tag{9}$$

2.3. Forces acting on a single flat-plate particle

Fig. 1 shows the dominant forces acting on a single flat-plate particle initially sedimented on the bottom wall of a rectangular duct in Poiseuille flow. The forces may be categorized into those acting parallel (horizontal) to the wall and those acting perpendicular (vertical) to the wall. The summation of the dominant horizontal forces is given by:

$$\sum \mathbf{F}_x = \mathbf{F}_\mathrm{D} - \mathbf{F}_\mathrm{F} \tag{10}$$

where $\mathbf{F}_\mathrm{D}$ is the drag force and $\mathbf{F}_\mathrm{F}$ is the friction force. The summation of the dominant vertical forces is given by:

$$\sum \mathbf{F}_y = \mathbf{F}_\mathrm{L} + \mathbf{F}_\mathrm{B} - \mathbf{F}_\mathrm{G} - \mathbf{F}_\mathrm{A} \tag{11}$$

where $\mathbf{F}_\mathrm{L}$ is the lift force, $\mathbf{F}_\mathrm{B}$ is the buoyancy force, $\mathbf{F}_\mathrm{G}$ is the gravity force, and $\mathbf{F}_\mathrm{A}$ is the adhesion force.

There are two potential modes of incipient motion for a non-spherical, flat-plate particle from rest: sliding or lifting (Hubbe, 1984;

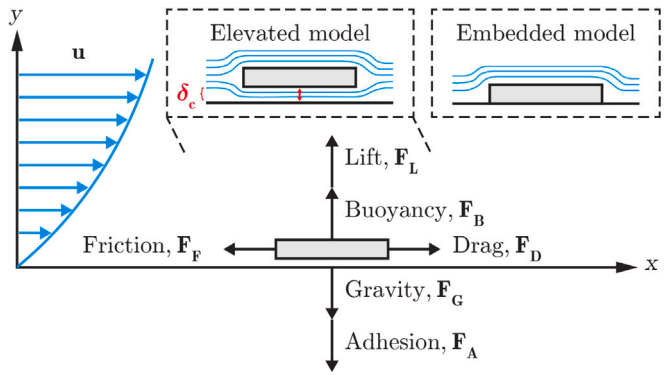

Fig. 1. Forces acting on a single flat-plate particle in Poiseuille flow through a rectangular duct. Encouraging forces to initiate particle motion and suspension include lift, buoyancy, and drag while resisting forces include gravity, adhesion, and friction. Accurate evaluations of drag and lift forces acting on the particle were made using computational simulations with an elevated model that provides a clearance, δ_c, between the particle and the wall boundary.

Rabinovich and Kalman, 2009b). The sliding mechanism occurs when the drag force overcomes the friction force. The lifting mechanism starts when the lift and buoyancy forces overcome the gravity and adhesion forces. The mode responsible for the incipient motion is the one for which the encouraging forces ($\mathbf{F}_D$, $\mathbf{F}_L$, $\mathbf{F}_B$) are greater than the resisting forces ($\mathbf{F}_F$, $\mathbf{F}_G$, $\mathbf{F}_A$) at the lowest fluid velocity. The adhesion forces include van der Waals and electrostatic forces. The van der Waals forces have been shown to be negligible for larger particles (Cabrejos and Klinzing, 1992).

2.4. Particle clearance with an elevated model

When employing numerical methods to evaluate the forces acting on a particle near a wall, appropriate placement of the particle needs to be considered. For numerical simulations of the flow around a moving particle with a moving fluidic mesh, contact of the particle and wall may pose convergence issues due to the topology change (Patankar et al., 2001). Even for numerical studies of the flow around a stationary particle, the particle–wall contact may lead to issues due to the singularity at the point of contact. Previous studies on lift of a spherical particle from a flat surface in shear flow highlighted problems in the evaluation of lift due to the singularity leading to local inaccuracies of the computed stresses (Krishnan and Leighton Jr., 1995). As shown in Fig. 1, there are two general approaches for particle placement to address the problems of particle–wall contact: an embedded model and an elevated model. Embedding the particle at different depths into the wall has previously been investigated in attempts to address the singularity issue for a contacting spherical particle (Martinez et al., 2009). However, the embedded model may provide a negative evaluated lift force due to the removal of the bottom particle surface where the pressure component of the lift force acts in the upward direction (Palakurthi et al., 2017). Alternatively, another approach involves providing a clearance distance, δ_c, between the particle and wall. The limiting case of a particle in contact with the wall may be approached by progressively decreasing δ_c (Leighton and Acrivos, 1985; Cherukat and Mclaughlin, 1994). However, small values for δ_c requires sufficiently high discretization for accurate computation of the flow field and stresses on the particle (Zeng et al., 2009; Lee and Balachandar, 2017).

2.5. Analytical solution of the average wall shear rate for flow through a finite rectangular channel

For characterization of the critical shear Reynolds number for hydrodynamic particle lift-off in rectangular microchannels, we evaluated the analytical solution of the average wall shear rate along the bottom surface of a channel, with channel height H, channel width W, and channel length L, in the absence of a particle. The fluid velocity profile along the x-direction, $U_x(y,z)$, has been previously derived for laminar flow of an incompressible, Newtonian fluid through a finite rectangular channel (Truskey et al., 2004):

$$U_x(y,z) = \frac{\Delta p H^2}{8\mu L}\left[\left(1-\frac{4y^2}{H^2}\right) - \sum_{n=0}^{\infty}\frac{32(-1)^n \cosh\left((2n+1)\pi z/H\right)\cos\left((2n+1)\pi y/H\right)}{(2n+1)^3\pi^3\cosh\left((2n+1)\pi W/2H\right)}\right] \tag{12}$$

where Δp is the pressure drop and μ is the fluid dynamic viscosity. The average wall shear rate along the bottom surface at $y=-H/2$ may then be calculated:

$$\langle\dot{\gamma}_w\rangle = \frac{\tau_{yx}}{\mu} = \frac{1}{W}\int_{-W/2}^{W/2}\left(\frac{\partial U_x}{\partial y}\bigg|_{y=-H/2}\right)dz = \frac{\Delta p H}{2\mu L}\left[1-16\left(\frac{H}{W}\right)\sum_{n=0}^{\infty}\frac{(-1)^n\tanh\left((2n+1)\pi W/(2H)\right)}{(2n+1)^3\pi^3}\right] \tag{13}$$

where τ_{yx} is the shear stress in the x-direction acting on the surface with its outward normal vector in the y-direction. The average wall shear rate in Eq. (13) is dependent on the pressure drop, Δp, but we can reexpress $\langle\dot{\gamma}_w\rangle$ as a function of the fluid flow rate, Q. The fluid flow rate is given by:

$$Q = 4\int_0^{W/2}\int_0^{H/2} U_x(y,z)\,dy\,dz \tag{14}$$

Following substitution, the average wall shear rate, which is used for evaluating the shear Reynolds number, may then be calculated using the following expression:

$$\langle\dot{\gamma}_w\rangle = \left(\frac{6Q}{H^2W}\right)\left[1-6\left(\frac{H}{W}\right)\sum_{n=0}^{\infty}\frac{\tanh\left((2n+1)\pi W/2H\right)}{(2n+1)^5\pi^5}\right]^{-1}\left[1-16\left(\frac{H}{W}\right)\sum_{n=0}^{\infty}\frac{(-1)^n\tanh\left((2n+1)\pi W/2H\right)}{(2n+1)^3\pi^3}\right] \tag{15}$$

3. Experimental methods

3.1. Dimensional analysis

An aim of the current study is to determine the fluid and channel variables affecting the critical lift-off mechanism of flat-plate, non-neutrally buoyant particles in horizontal channels with a rectangular cross-section:

$$f\left(d,\rho_p,H,W,D_H,\mu,\rho_f,\langle U\rangle,\langle\dot{\gamma}_w\rangle,g\right)=0 \tag{16}$$

where the functional relationship f must be independent of a specific system of units (Gibbings, 2011). Through nondimensionalization using the Buckingham π theorem (Buckingham, 1914; Karam and Saad, 2021), the above expression may be restated as a relationship F, in terms of dimensionless π groups:

$$F\left(\frac{H}{d},\frac{W}{d},\frac{d}{D_H},\frac{\rho_p}{\rho_f},\frac{\rho_p{}^2\,g d^3}{\mu},\frac{\rho_f\langle U\rangle D_H}{\mu},\frac{\rho_f\langle\dot{\gamma}_w\rangle d^2}{\mu}\right)=0 \tag{17}$$

where the sixth π group is the channel Reynolds number and the seventh π group is the shear Reynolds number. It can be observed that the third and sixth π groups may be manipulated to provide the particle Reynolds number. Also, through manipulation of the fourth and fifth π groups, the Archimedes number may be found. While dimensional analysis revealed the potential significance of the channel-particle size parameters, H/d and W/d, in affecting the particle lift-off, the two π groups may also be manipulated to account for the possibility of the channel cross-sectional area, $A=HW$, and the aspect ratio, H/W, also being significant parameters. From application of dimensional analysis, the critical shear Reynolds number, $\check{\mathrm{R}}\mathrm{e}_{s,d}$, necessary for lift-off of a

Table 1
Physical properties of the flat-plate particle and fluids for particulate microchannel flow studies at 25 °C.

	Material	Density, ρ (kg/m^3)	Dynamic viscosity, μ (Pa s)	Relative permittivity, ϵ_r (–)
Solid particle	p-Chip	2329	–	–
Fluid phase	Isopropyl alcohol	785	2.07×10^{-3}	19.92
	Water	997	8.89×10^{-4}	78.39
	Methanol	792	5.40×10^{-4}	32.70

single flat-plate particle in horizontal, rectangular channels, may then be formulated to be dependent on the following parameters:

$$\check{\mathrm{Re}}_{s,d} = F\left(\frac{H}{d}, \frac{W}{d}, \frac{HW}{d^2}, \frac{H}{W}, Ar_d, Re, Re_{p,d}\right) \tag{18}$$

3.2. Particle and fluids

A 600 μm × 600 μm × 100 μm p-Chip microtransponder (p-Chip Corporation, Chicago, IL, USA) was used as a representative flat-plate, non-neutrally buoyant microchip particle for the single particle lift-off studies. The properties of p-Chips have been previously described by Gruda et al. (2010), Li et al. (2010), Lin et al. (2007), Mandecki et al. (2006) and Rich et al. (2012). The p-Chip is a non-uniform, composite object fabricated using a planar semiconductor manufacturing process from silicon wafers that have been deposited and patterned with layers of polysilicon and silicon dioxide, and diced into individual microchips. Since the deposited layers are relatively thin compared to the thickness of the underlying silicon, we considered the p-Chip as a uniform particle with properties of silicon for our analysis.

One of the major surfaces of the p-Chip contains integrated circuits, microfeatures that may affect the friction along the surface. From inclined plane tests, we determined that the difference between the particle–wall kinetic friction coefficients, μ_{kf}, with respect to the two major particle surfaces was insignificant (Appendix A). As a result, the non-uniformity of the surfaces of the p-Chip has a negligible effect on the observed flow conditions for particle lift-off. Based on previous studies of particulate flow in poly(methyl methacrylate) (PMMA) channels for non-spherical sand of the same size range as the p-Chip, we assumed the value of 0.70 for the static friction coefficient, μ_{sf}, between the particle and wall (Rabinovich and Kalman, 2009a) for the calculation of the modified Archimedes number in Eq. (8). Isopropyl alcohol, deionized water, and methanol (Sigma-Aldrich, St. Louis, MO, USA), each with different kinematic viscosities, were chosen as solvents for the particulate flow studies. The physical properties of the particle and fluids are summarized in Table 1.

3.3. Channel fabrication and experimental setup

A 3^2 central composite face-centered (CCF) design with replicated center points was used to construct the design of experiments outlining the configurations for the rectangular channel, with different channel heights (H) and channel widths (W) used for the particulate flow studies. Three levels were chosen for each of the two factors considered: channel aspect ratio, H/W, and width domain size, W/d_{max}. An additional experimental design point (H: 1.50 mm, W: 1.00 mm) was added to investigate the effect of the channel aspect ratio on the critical lift-off behavior. Table 2 presents all the channel configurations used in the current experimental and computational lift-off studies. The dimensions presented in the study are the dimensionally accurate values ± 0.03 mm.

The design and features of the microfluidic manifold are illustrated in Fig. 2. Designs of the microchannels were created in the vector graphics software, Adobe Illustrator 2023 (Adobe Inc., San Jose, CA). To fabricate the chip, we machined PMMA sheets using a desktop computer numerical control (CNC) mill (Bantam Tools Desktop PCB Milling Machine, Peekskill, NY, USA). The PMMA sheets were sealed to form rectangular microchannels using an ethanol-assisted thermal bonding process (Liga et al., 2016). Custom fluidic adapters with an integrated physical particle trap were designed using SOLIDWORKS 2022 (Dassault Systèmes, Waltham, MA, USA) and 3-D printed using the Form 3B stereolithography printer with Formlabs Clear v04 resin (Formlabs, Somerville, MA, USA). Fine features of the device were fabricated at the resolution of 25 μm for both the CNC mill and 3-D printer.

A fluidic adapter was directly interfaced to both the inlet and outlet of the PMMA microchannel to allow for horizontal fluid flow delivery to the microfluidic device while keeping the microchip particle contained within the manifold. Viton™ fluoroelastomer O-rings (The Chemours Company, Wilmington, DE, USA) were added in between conduit interfaces to achieve a fluidic seal. A horizontally-oriented fluidic adapter, with the inlet parallel to the channel length, was chosen over a perpendicular interconnection to eliminate corner vortices that could indefinitely trap the particle. The design of the physical particle trap, which had a circular cross-section containing three equally-spaced circular through holes (0.7 mm in diameter) in a radial pattern, allowed for sufficient resin clearance during component fabrication and also facilitated flow stabilization during the particulate flow experiments. The size and orientation of the circular cross-section of the particle trap were held constant for all tested channel configurations. The bottom point of the circular surface of the trap was coincident with the bottom channel plane. The circular surface of the particle trap was lofted to the rectangular surface of the channel for each experimental configuration. The nominal channel length was 200 mm.

Fig. 3 shows the experimental assembly for the particulate flow experiments to evaluate the critical flow rates for microchip particle lift-off. Alignment of the microfluidic manifold was maintained using integrated Maxwell kinematic couplings between the device adapters and the base mount (Slocum, 2010). Fluid was delivered to the microchannel at set constant flow rates using a syringe pump (Model 44, Harvard Apparatus, Holliston, MA USA). The syringe pump, connected to a computer through an RS-232 interface, was controlled using a custom LabVIEW virtual instrument (VI) program (NI LabVIEW 2020, Austin, TX, USA). A top-mounted, USB 3.0, 1.3 MP, monochrome camera (MQ013MG-ON, Ximea, Münster, Germany) with an attached lens configuration (MVL6X12Z, MVL20 A, MVLCMC, MVL6X025L, MVL05 A; Thorlabs, Newton, NJ, USA) was used to capture video recordings (at 1500 frames per second) of the particle motion along the xz-plane coincident with the channel width and length. A 10K lux LED panel was mounted at the bottom of the transparent channel to provide uniform lighting and achieve fast image acquisition. The field of view of the camera encompasses the transparent PMMA channel downstream of the translucent particle trap inlet.

3.4. Particle lift-off experiments

A single p-Chip was loaded into the microfluidic manifold and encapsulated between the particle traps. A programmed sequence from the LabVIEW VI was used to flow the single p-Chip, at a specified constant flow rate and at room temperature of 25 °C, in a forward–backward cycle with a brief pause between each state transition to allow sufficient time for the flow system to stabilize and for the p-Chip to settle near the inlet particle trap prior to collection of lift-off data. Videos of the flowing p-Chip, initially sedimented adjacent to the inlet particle trap, were collected at various constant fluid flow rates. For each experimental configuration with a particular solvent, channel design, and operating fluid flow rate, five experimental trials were performed to determine the critical volumetric flow rate nec-

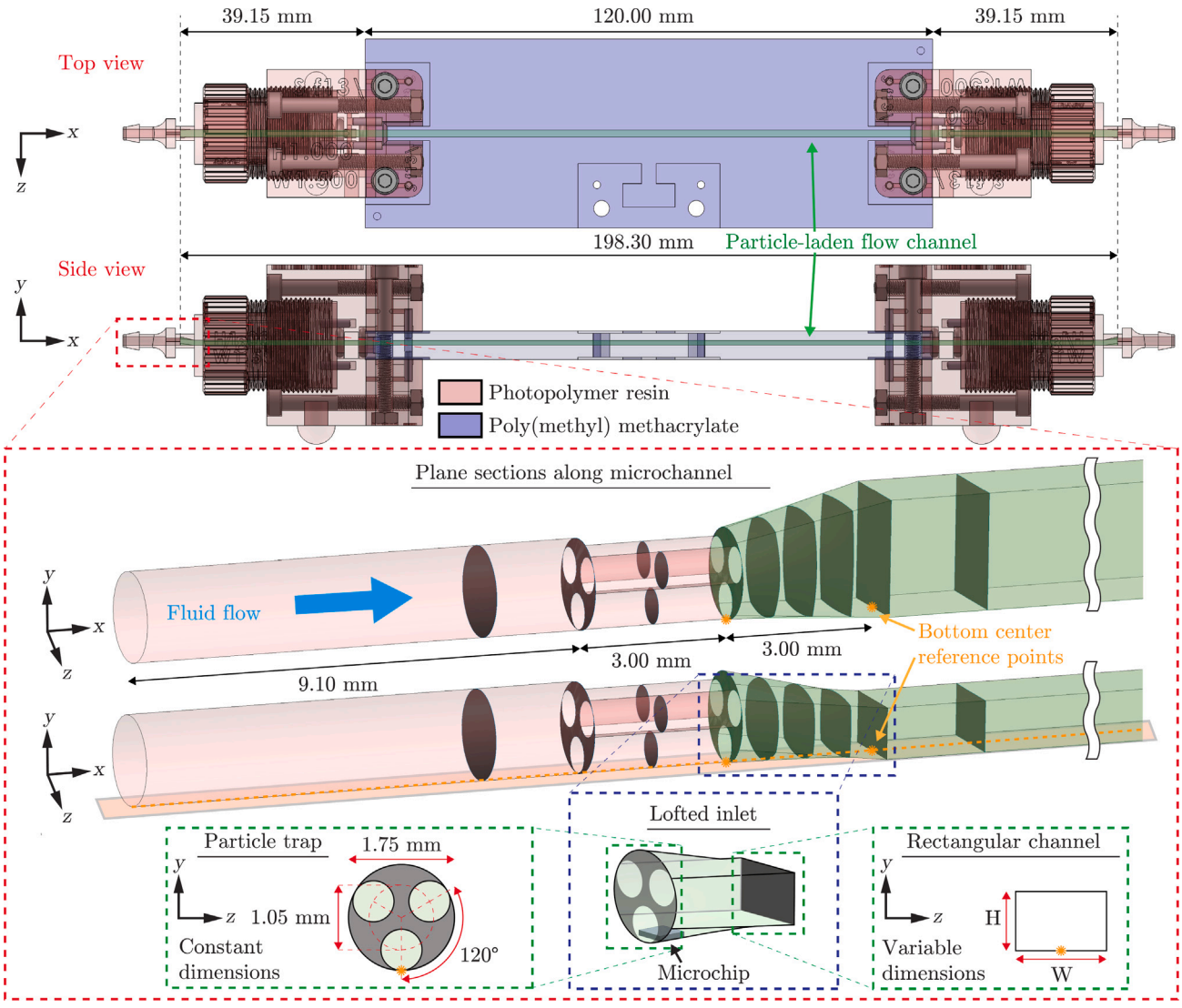

Fig. 2. Design of the straight rectangular microchannel device for experimental particulate flow studies of lift-off of a single flat-plate microchip particle sedimented at the inlet near a physical particle trap containing three through holes. Experimental lift-off fluid flow rates were assessed for all combinations of fluid solvents, and channel configurations with different channel areas and aspect ratios.

Table 2
Experimental configurations for the microchannels with rectangular cross-sections.

Experimental characterization						
Configuration	Channel dimensions (mm)		Channel aspect ratio (–)	Channel-particle domain size parameters (–)		
	H	W	H/W	W/d_{max}	H/d_{max}	HW/d_{max}^2
1	1.00	1.50	0.67	1.77	1.18	2.1
2	1.50	1.00	1.50	1.18	1.77	2.1
3	1.50	1.50	1.00	1.77	1.77	3.1
4	0.89	1.33	0.67	1.57	1.05	1.6
5	1.33	1.33	1.00	1.57	1.57	2.5
6	1.13	1.70	0.67	2.00	1.33	2.7
7	2.26	1.70	1.33	2.00	2.67	5.3
8	1.78	1.33	1.33	1.57	2.09	3.3
9	2.00	1.50	1.33	1.77	2.36	4.2
10	1.70	1.70	1.00	2.00	2.00	4.0

essary for lift-off. The critical flow rate for particle lift-off at each experimental configuration was defined to be the flow rate (probed at 1 mL/min steps) necessary for steady particle movement among all five experimental trials. The experiments were performed for all combinations of solvents (isopropyl alcohol, water, and methanol) and channel configurations defined in Table 2. The data was analyzed using MATLAB 2023a (MathWorks, Natick, MA, USA).

4. Computational methods

4.1. Numerical models of single particle microchannel flow

To gain insight into the hydrodynamic forces acting on the flat-plate particle at the experimentally observed critical fluid flow rates and to assess the effects of the particle trap on the hydrodynamic

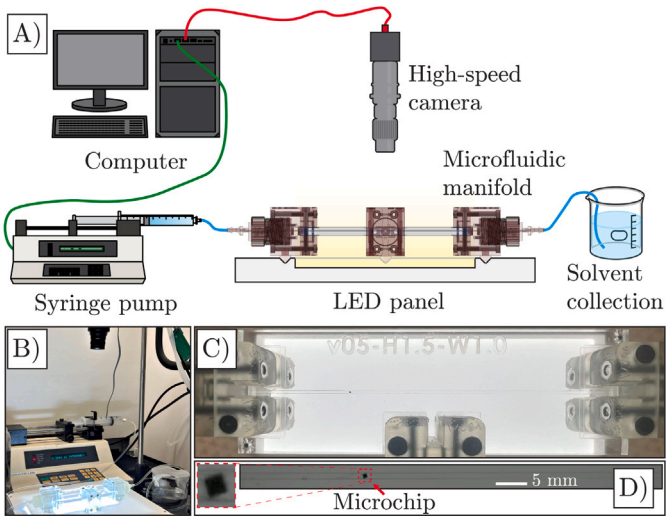

Fig. 3. Experimental assembly for the characterization of microchip particle lift-off. (A) Schematic of the assembly for characterizing the lift-off of a single flat-plate particle initially sedimented near the inlet of a microfluidic channel. The minimum flow rate for lift-off of the particle was recorded for each of the experimental configurations with different channel and solvent combinations. (B) Camera image of the experimental particulate flow setup. (C) Top-down camera image of an illuminated channel from a specific configuration (H = 1.50 mm, W = 1.00 mm). (D) Full frame from a recorded video (H = 1.50 mm, W = 1.00 mm, Q = 7 mL/min) of the flowing microchip particle.

forces acting on the particle, we performed CFD simulations of the steady-state fluid flow around a single, stationary, sedimented, flat-plate particle located near the bottom channel wall and at different lengths along the axial channel centerline. A finite element method was implemented using the COMSOL Multiphysics® software with the CFD Module (COMSOL, Inc., Burlington, MA, USA) to numerically solve the continuity and Navier–Stokes equations for a laminar flow model of an incompressible, Newtonian fluid of constant density. Since we are investigating the forces leading to the incipient motion of a particle initially at rest, a stationary solver was used to resolve the steady-state flow. The simulations considered only the fluid domain; the solid particle was modeled as a void volume within the fluid domain. The fluid flow around a single particle sedimented on the bottom wall is more appropriately expressed using an elevated model that accounts for stresses on the bottom surface of the particle (Palakurthi et al., 2017). Therefore, we specified a clearance distance of δ_c between the particle and the channel wall.

4.2. Governing equations

The steady-state laminar flow of an incompressible, Newtonian fluid with an external gravity force in the negative y-direction was modeled using the following forms of the Navier–Stokes and continuity equations, respectively:

$$\rho_f(\mathbf{u}\cdot\nabla)\mathbf{u} = \nabla\cdot\boldsymbol{\sigma} + \rho_f\mathbf{g} \tag{19}$$

$$\rho_f\nabla\cdot\mathbf{u} = 0 \tag{20}$$

where ρ_f is the fluid density, $\mathbf{u}$ is the fluid velocity vector, and $\mathbf{g}$ is the gravitational field. The total stress tensor, $\boldsymbol{\sigma}$, is composed of the pressure component, $-p\mathbf{I}$, and viscous stress tensor, $\boldsymbol{\tau}$:

$$\boldsymbol{\sigma} = -p\mathbf{I} + \boldsymbol{\tau} \tag{21}$$

where p is the pressure and $\mathbf{I}$ is the identity matrix. The viscous stress tensor, $\boldsymbol{\tau}$, is given by:

$$\boldsymbol{\tau} = \mu_f\left(\nabla\mathbf{u} + (\nabla\mathbf{u})^T\right) \tag{22}$$

where μ_f is the dynamic viscosity of the fluid and T is the transpose. The forces acting on the particle are evaluated by integrating the total stress contributions around the entire particle surface, S. The drag force, which considers all the tangent, x-directional stresses, and the lift force, composed of the normal, y-directional stresses, may then be evaluated by:

$$\mathbf{F}_D = \int_S \mathbf{n}_x\cdot\boldsymbol{\sigma}\,dS \tag{23}$$

$$\mathbf{F}_L = \int_S \mathbf{n}_y\cdot\boldsymbol{\sigma}\,dS \tag{24}$$

where $\mathbf{n}_x$ and $\mathbf{n}_y$ are the outward unit normal in the x-direction and y-direction, respectively.

4.3. Computational domain, boundary conditions, and mesh

Since the experimental characterization of lift-off of a single flat-plate particle was performed with the particle at rest near the inlet consisting of a lofted particle trap, the entrance effects on lift-off needed to be investigated. To evaluate the hydrodynamic forces acting on the particle to initiate lift-off, we performed computational simulations using the fluidic domain of each configuration of the particle trap adapter where the particle initially begins at rest. The distance from the particle trap cross-section to the outlet of the computational domain was 33.18 mm. Since the channel exhibits symmetry about the xy-plane, we performed CFD simulations on half of the full channel geometry. A constant flow rate corresponding to half of the experimentally observed critical flow rate needed for lift-off was applied as the inlet boundary condition. A constant atmospheric pressure boundary condition was set at the outlet. The no-slip boundary condition was applied for all the walls and particle surfaces. The reported values for the evaluated drag and lift forces correspond to that acting on a full (non-halved) particle. Free tetradehedral mesh elements were used for the fluidic domain and hexahedral mesh elements with further mesh refinement are used for the boundary layers.

For some configurations, the entrance length $L_e = 0.058D_H\mathrm{Re}$ (Bergman, 2011) beyond which the flow is fully developed, was estimated to be greater than the length of the computational domain of the imported channel adapter. As a result, fully-developed models with a stationary particle situated in the middle of a 2 mm length channel were also performed to evaluate the hydrodynamic forces downstream.

A mesh independence study, based on the evaluated drag and lift forces at the experimentally observed critical flow rates, was performed to determine the appropriate mesh settings and to ensure the numerical solutions for the hydrodynamic forces do not change significantly with further mesh refinement. The configurations for the mesh considered in the mesh independence study included minimum boundary element sizes ranging from 637 μm to 2.55 μm. The mesh independence study was conducted with the channel configuration with the smallest features (H = 0.89 mm, W = 1.33 mm) providing the highest flow gradients. Forces at the different axial positions of the particle (ΔL_p = 0.10, 0.90, 2.40, 3.01, 23.00 mm) were evaluated to ensure the computed results do not change with particle positioning, or length steps. Following selection of the appropriate mesh configuration, an assessment of the effect of the clearance distance, δ_c, between the bottom particle surface and the bottom channel wall on the evaluated hydrodynamic forces, was performed. The main parameters used in the simulations are summarized in Table 3.

4.4. Parametric computational studies and particle positioning

Preparation of the computational particulate flow simulations included several requirements: (1) construction of parametric geometries corresponding to the different microchannels investigated, (2) configurable placement of the particle at various distances from the bottom channel wall and from the channel inlet, and (3) precise positioning

Table 3
Parameters used for computational simulations of a single, stationary flat-plate particle in straight rectangular microchannel flows.

Numerical simulation		
Parameter	Definition	Value(s)
δ_c	Clearance between bottom of particle and bottom channel wall (mm)	0.05
ΔL_p	Axial distance of particle from inlet (mm)	0.10, 0.90, 2.40, 3.01, 23.00
$e_{ng,max}$	Global maximum element size (mm)	0.854
$e_{ng,min}$	Global minimum element size (mm)	0.255
$e_{nb,max}$	Boundary maximum element size (mm)	0.471
$e_{nb,min}$	Boundary minimum element size (mm)	0.051
e_{num}	Average number of elements	$73\,900 \pm 600$

of the flat-plate particle in relation to the complex geometry of the particle trap containing curved, lofted walls. Therefore, we used SOLIDWORKS to construct the designs of the channel configurations and define configurable relations between the particle and channel features, the LiveLink™ for SOLIDWORKS module (COMSOL, Inc., Burlington, MA, USA) to import the configurable parameters into COMSOL, and COMSOL to perform the parametric particulate flow simulations for all channel and fluid flow configurations.

Computer-aided design of each microchannel was prepared as a configuration within SOLIDWORKS. The orientation of the particle was constrained such that the particle xy-midplane, located between two minor surfaces of the flat-plate particle, remained coincident with the channel xy-midplane situated between the side channel walls. For precise orientation of the flat-plate particle in relation to the inlet and the bottom channel wall, reference lines were mounted on the particle. The particle distance, ΔL_p, the axial distance between the particle and inlet, is defined by the length of an outward reference line that is perpendicular to the minor surface of the particle. The endpoints of this reference line are coincident to the centroid of the minor particle surface and the channel inlet surface, respectively. The clearance distance, δ_c, the distance between the bottom, major particle surface and the bottom channel wall, is defined as the length of the outward reference lines that are perpendicular to the major particle surface. These reference lines originate from the corners of the major particle surface and the other endpoints of the lines are coincident with the bottom channel wall. Fig. 4 shows the computational domain, boundary conditions, mesh, and particle positioning.

5. Results and discussion

5.1. Experimental flat-plate particle lift-off

Figs. 5 and 6 present the observed critical shear Reynolds number, $\check{\mathrm{Re}}_{s,d_{max}}$, as a function of the Archimedes number, $\mathrm{Ar}_{d_{max}}$, for all ten channel configurations and three solvents tested. The results for a flat-plate particle with $\mathrm{Ar}_{d_{max}}$ ranging from 1700 to 25 000 were compared to that from a separate numerical study for a spherical particle with $\mathrm{Ar}_{d_{max}}$ ranging from 2 to 6363 (Patankar et al., 2001). It is noted that the different $\mathrm{Ar}_{d_{max}}$ reported for the current particle lift-off studies for a flat-plate particle reflect only the changes in the solvent properties since a single type of particle was considered in the study. As was observed from previous findings for a spherical particle, it is observed that greater $\check{\mathrm{Re}}_{s,d_{max}}$ is required to lift the flat-plate particle at higher $\mathrm{Ar}_{d_{max}}$.

At each $\mathrm{Ar}_{d_{max}}$ considered in the experimental particulate flow studies for a flat-plate particle, an increase in the height domain size, H/d_{max}, resulted in a lower $\check{\mathrm{Re}}_{s,d_{max}}$ for lift-off. Patankar et al. (2001) showed that the $\check{\mathrm{Re}}_{s,d_{max}}$ for a spherical particle at different $\mathrm{Ar}_{d_{max}}$ may

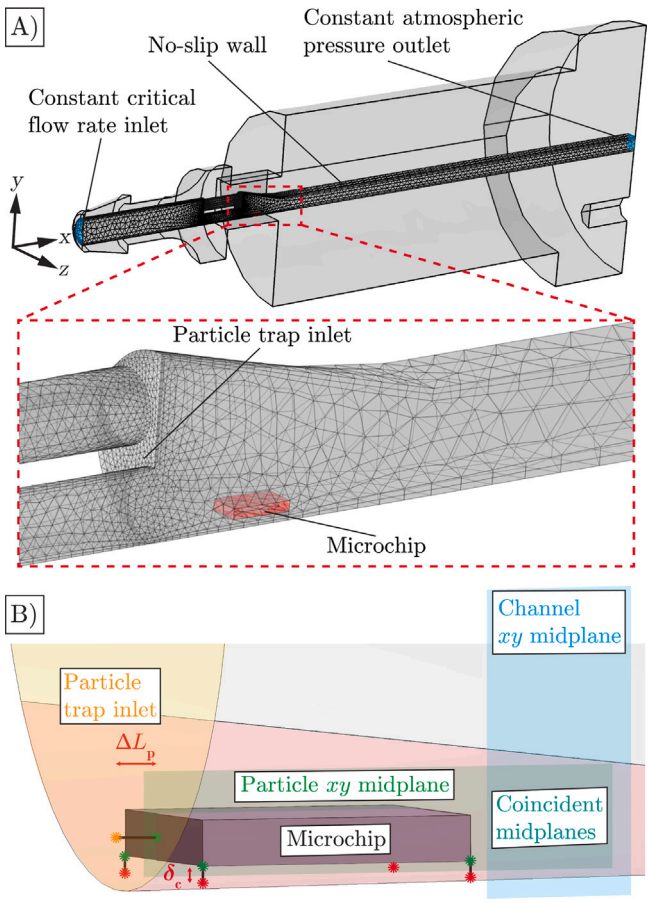

Fig. 4. Computational domain, boundary conditions, mesh, and particle position for the numerical simulations to evaluate the hydrodynamic drag and lift forces acting on a single flat-plate microchip particle initially sedimented near the microchannel inlet. The channel configuration shown corresponds to that for $H = 1.00$ mm, $W = 1.50$ mm, $\delta_c = 0.05$ mm, $\Delta L_p = 0.90$ mm. (A) Computational fluid domain corresponding to a halved model of the particle trap adapter containing a pseudo-particle modeled as a void volume. (B) Schematic of the positioning of the particle in the simulations with the following configurable parameters: the axial distance of the particle from the inlet, ΔL_p, and clearance distance between the bottom particle surface and the bottom channel wall, δ_c.

be modeled using an empirical power law equation for each H/d_{max} considered. Fig. 5 shows the $\check{\mathrm{Re}}_{s,d_{max}}$ for a flat-plate particle at different $\mathrm{Ar}_{d_{max}}$ and H/d_{max} are within the range of values from the extrapolated power law equations from Patankar et al. (2001). However, the values of H/d_{max} for a flat-plate particle were significantly lower than that for a spherical particle for the relationship between $\check{\mathrm{Re}}_{s,d_{max}}$ and $\mathrm{Ar}_{d_{max}}$.

We also observed the experimentally characterized relationship between $\check{\mathrm{Re}}_{s,d_{max}}$ and $\mathrm{Ar}_{d_{max}}$ for the flat-plate particle deviated from the power law models formulated from numerical simulations for a spherical particle (Patankar et al., 2001). Since the previous numerical simulations from Patankar et al. (2001) did not account for adhesion forces, the deviations from the present study suggest that for this relatively large microchip particle, electrostatic adhesion forces may significantly affect the lift-off behavior.

In addition, the area domain size, HW/d_{max}^2, which was determined through dimensional analysis to be a potential channel-particle size parameter affecting $\check{\mathrm{Re}}_{s,d_{max}}$, was shown to be a more appropriate parameter than H/d_{max} (Patankar et al., 2001; Hur et al., 2011) to capture the effects of the channel-particle size in three-dimensions. The comparison of the lift-off for a flat-plate particle and a spherical particle revealed similarities in the lift-off behavior but also showed that characterization studies and models for lift-off of spherical particles

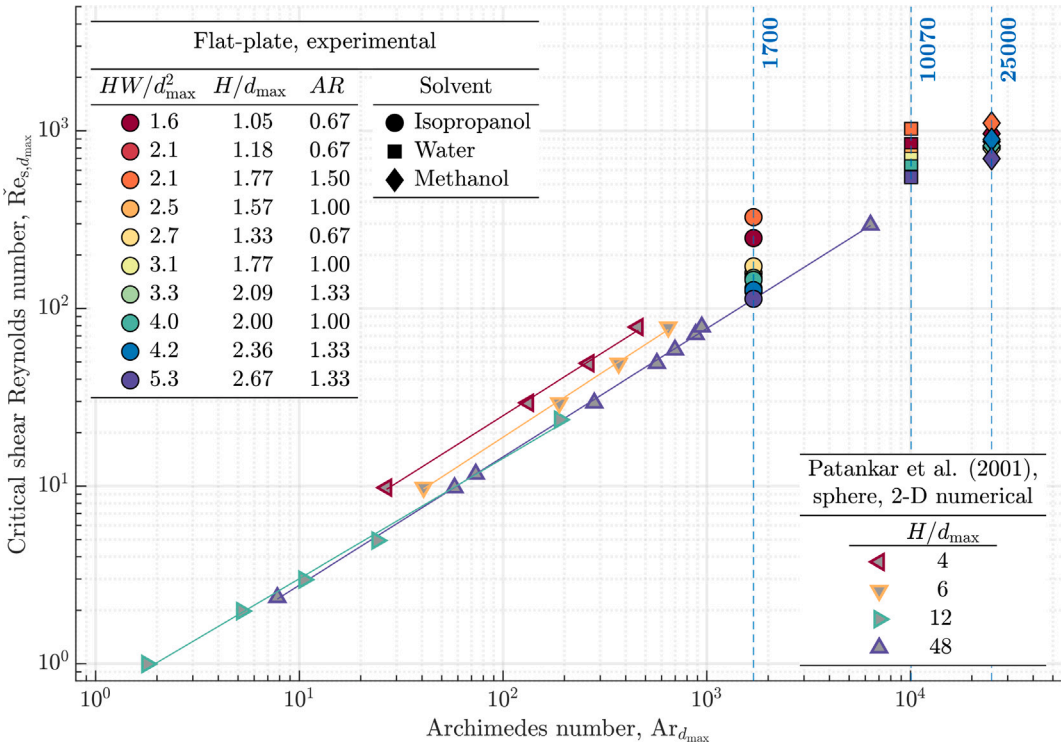

Fig. 5. Effect of the Archimedes number, $\mathrm{Ar}_{d_{max}}$, and channel-particle domain sizes, H/d_{max} and HW/d_{max}^2, on the critical shear Reynolds, $\check{\mathrm{Re}}_{s,d_{max}}$, for particle lift-off. The experimental data for lift-off of a flat-plate particle is compared to 2-D ALE numerical data for lift-off of a spherical particle (Patankar et al., 2001). The range of values for H/d_{max} needed for lift-off of a flat-plate particle is significantly lower than that evaluated from planar numerical studies for a spherical particle, suggesting relationships for lift-off of a spherical particle may not be directly applied to an aspherical, flat-plate particle without additional corrections. Both the height domain size, H/d_{max}, and the area domain size, HW/d_{max}^2, affects $\check{\mathrm{Re}}_{s,d_{max}}$. However, HW/d_{max}^2 appropriately captures the 3-D contributions of the channel dimensions to the flow profile around the particle. While the relationship between $\mathrm{Ar}_{d_{max}}$ and $\check{\mathrm{Re}}_{s,d_{max}}$ for a spherical particle was previously determined to follow an empirical power law model for each channel-particle domain size, it is noted that the current flat-plate particle lift-off data deviates from the extrapolated linear relationships. The deviation suggests electrostatic effects, which are not considered in the previous ALE study, significantly affect lift-off.

cannot be used to accurately predict the lift-off of non-spherical, flat-plate particles. It is noted that although the lift-off results are discussed with respect to HW/d_{max}^2 and H/d_{max}, these results effectively reflect only the effect of the channel dimensions on lift-off since d_{max} remains constant for the single type of flat-plate particle considered.

In Fig. 6, the experimental data for $\check{\mathrm{Re}}_{s,d_{max}}$ and $\mathrm{Ar}_{d_{max}}$ was categorized in terms of the channel aspect ratio, H/W. We observed at each investigated $\mathrm{Ar}_{d_{max}}$ that an increase in HW/d_{max}^2 resulted in a decrease in $\check{\mathrm{Re}}_{s,d_{max}}$ for $H/W \neq 1$. For $H/W = 1$, changes in HW/d_{max}^2 did not significantly affect the observed $\check{\mathrm{Re}}_{s,d_{max}}$. The findings revealed that accurate prediction of $\check{\mathrm{Re}}_{s,d_{max}}$ at each $\mathrm{Ar}_{d_{max}}$ must consider both the area domain size, HW/d_{max}^2, and the channel aspect ratio, H/W.

5.2. Mesh independence results

The results of the mesh independence study are summarized in the Supplementary Material in Appendix A. Comparison of the results from successive mesh designs with minimum boundary element sizes, $e_{nb,min}$, of 19 μm and 51 μm at different axial particle positions, or length step, yielded mean, relative percentage errors (± SE) of $-2 \pm 1\%$ and $-0.1 \pm 0.5\%$ for the evaluated lift and drag forces, respectively. The error in the evaluated hydrodynamic forces remained minimal for each length step. Therefore, the mesh configuration with $e_{nb,min}$ of 51 μm was used for the simulations. For the assessment of an appropriate clearance distance, evaluated hydrodynamic forces were compared for simulation configurations with clearance distances, δ_c, of 0.01, 0.05, and 0.1 mm (Appendix A). Changing δ_c from 0.1 to 0.05 mm resulted in mean percentage refinement (± SE) in the lift and drag forces of $8 \pm 4\%$ and $-20.4 \pm 0.7\%$, respectively. While further refinement in both the mesh and clearance distance was possible for some experimental channel and solvent configurations, certain cases yielded convergence issues related to the sliver faces and other small features. Therefore, the clearance distance $\delta_c = 0.05$ mm was used for all the computational simulations.

5.3. Simulation of hydrodynamic forces on particle

Fig. 7 shows the computational particulate flow domain and numerically evaluated velocity profile around the stationary particle for one configuration ($H = 1.00$ mm, $W = 1.50$ mm, $\delta_c = 0.05$ mm, $\Delta L_p = 0.90$ mm) from the steady-state CFD studies. Both embedded and elevated particle models were investigated in the numerical simulations for evaluating the hydrodynamic forces. However, consistent with previous studies on spherical particle detachment (Palakurthi et al., 2017), an embedded flat-plate particle model yielded unrealistic, negative magnitudes for the evaluated lift forces. Evaluation of the forces on each of the six particle surfaces revealed that the lift forces acting on the particle are dominated by the pressure contributions to the top and bottom surfaces. As shown from the velocity profiles with streamlines around the particle, the current elevated particle model appropriately resolves the contributions of the forces on the bottom surface.

Fig. 8 presents the evaluated lift forces acting on the flat-plate particle from the fully-developed CFD studies with a stationary particle positioned at various axial distances along the channel. The data is categorized and presented in terms of the different configurations of the channel aspect ratio (H/W) and the solvent. For all configurations investigated, the flat-plate particle experienced elevated lift forces at the region near the inlet particle trap. However, as the particle was positioned further downstream, the magnitudes of the lift forces decayed. Interestingly, for all configurations of the computational studies, which

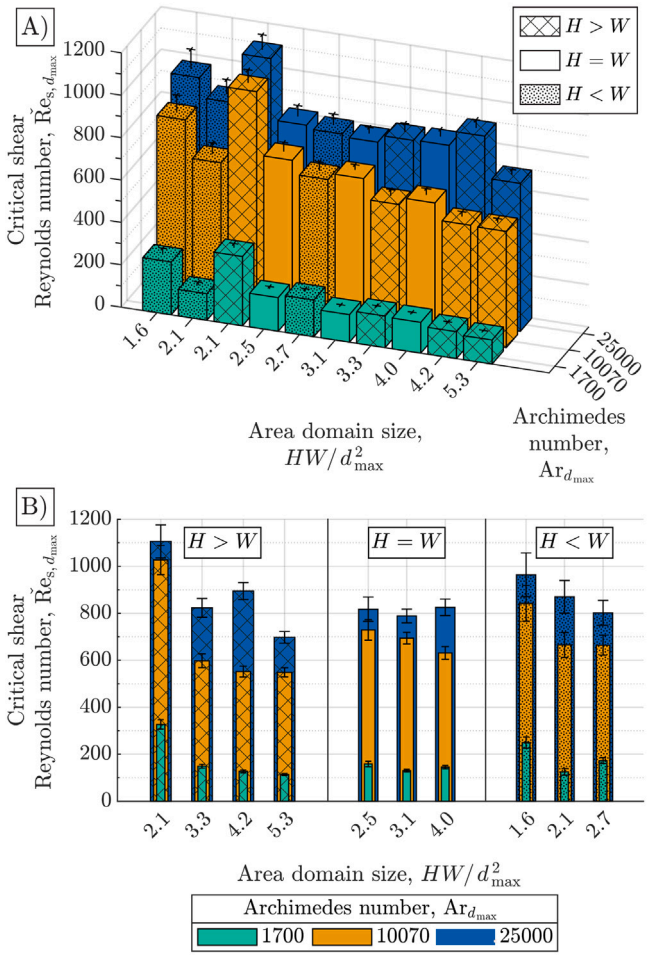

Fig. 6. Experimentally characterized lift-off of a flat-plate particle at different Archimedes number, $\mathrm{Ar}_{d_{max}}$, area domain sizes, HW/d^2_{max}, and channel aspect ratios, H/W. (A) The critical shear Reynolds number, $\check{\mathrm{Re}}_{s,d_{max}}$, as a function of HW/d^2_{max} and $\mathrm{Ar}_{d_{max}}$. At each $\mathrm{Ar}_{d_{max}}$, higher HW/d^2_{max} generally reduced the $\check{\mathrm{Re}}_{s,d_{max}}$, but HW/d^2_{max} alone cannot accurately predict $\check{\mathrm{Re}}_{s,d_{max}}$. (B) Effect of HW/d^2_{max} and $\mathrm{Ar}_{d_{max}}$ at different H/W. At each considered $\mathrm{Ar}_{d_{max}}$, an increase in HW/d^2_{max} resulted in a decrease in $\check{\mathrm{Re}}_{s,d_{max}}$ for $H/W \neq 1$. For $H/W = 1$, changes in HW/d^2_{max} did not significantly affect the observed $\check{\mathrm{Re}}_{s,d_{max}}$.

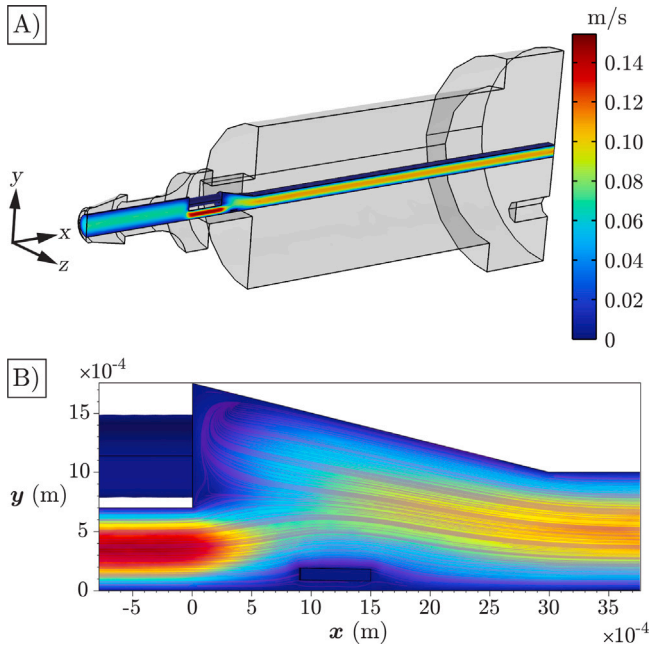

Fig. 7. Numerically evaluated velocity profile with streamlines along the fluidic adapter and around the stationary particle for one of the channel configurations (H = 1.00 mm, W = 1.50 mm, δ_c = 0.05 mm, ΔL_p = 0.90 mm). (A) 3-D fluid velocity profile through the fluidic domain of the fluidic adapter. (B) xy-view of the fluid velocity profile with streamlines around the particle. The steady-state CFD study with the elevated particle appropriately considered the contributions of the stresses on the bottom surface of the particle to the total hydrodynamic forces acting on the particle.

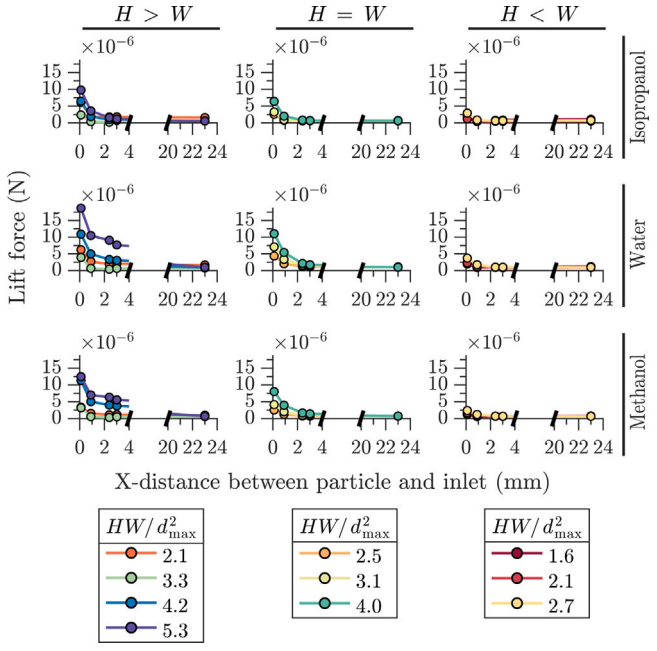

Fig. 8. Evaluated lift forces acting on the flat-plate particle from steady-state computational models with a stationary particle at various axial distances along the channel. The evaluated forces are shown for different configurations of channel aspect ratios (H/W) and solvent. The particle experienced elevated lift forces along the entrance of the inlet particle trap. However, the magnitudes of the lift forces evaluated with the particle downstream for all experimental configurations showed a strong convergence towards a singular value of $(6.7 \pm 0.4) \times 10^{-8}$ N indicating the particle remained suspended after lift-off.

employ the experimentally observed critical flow rates for flat-plate particle lift-off as a constant inlet boundary condition, the lift forces converged to a singular value of $(6.7\pm0.4)\times10^{-7}$ N when the particle was positioned beyond the entrance length, L_e. Previous studies on visual observations of the incipient motion of spherical and non-spherical particles in horizontal particle–fluid systems revealed that spherical particles begin their motion by rolling while non-spherical particles (larger than 0.4 mm in diameter) start their motion by sliding (Sharma et al., 1992; Rabinovich and Kalman, 2009a). While the results are insufficient for determining whether the incipient motion of the particle from rest begins with sliding or lifting, the findings reveal the particle remains suspended during saltation, or following initial particle suspension.

The drag forces acting on the flat-plate particle, positioned along the channel length, were also evaluated and presented in Fig. 9. As was observed for the lift forces, the drag forces acting on the particle were elevated in the region near the inlet particle trap and decayed rapidly as the particle was positioned further along the channel length. However, evaluation of the drag forces with the particle positioned downstream of L_e presented a range of values from 5.9×10^{-7} to 2.9×10^{-6} N among all study configurations. The findings further indicate that following initial suspension, the transported particle remains suspended rather than sliding along the channel.

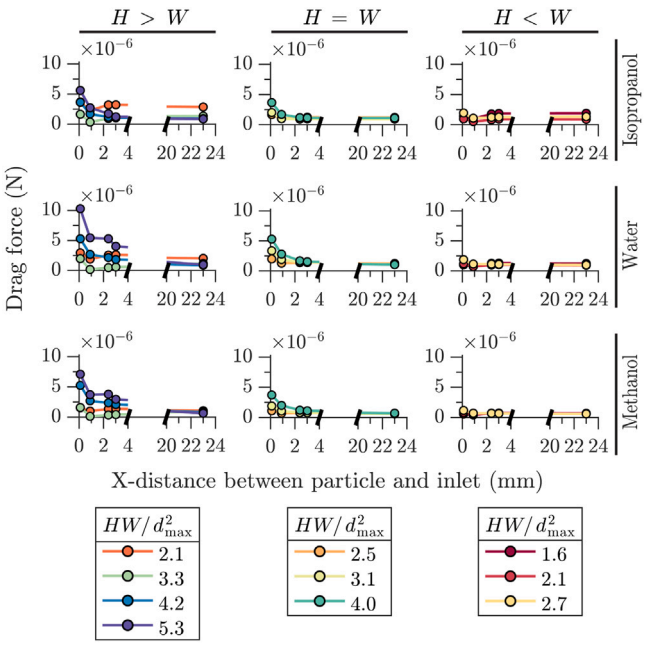

Fig. 9. Evaluated drag forces acting on the flat-plate particle from steady-state computational models with a stationary particle at various axial distances along the channel. The evaluated forces are shown for different configurations of channel aspect ratios (H/W) and solvent. The flat-plate particle generally experiences elevated drag forces along the entrance of the inlet particle trap. The magnitudes of the drag forces evaluated with the particle downstream for all experimental configurations do not all converge to a single value suggesting the particle does not slide along the bottom channel after lift-off.

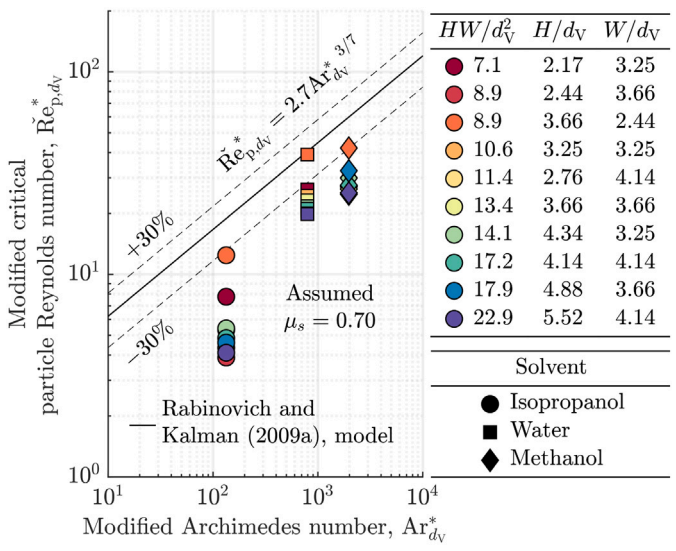

Fig. 10. Experimental data for single flat-plate particle lift-off mapped onto a generalized curve (Rabinovich and Kalman, 2009a) for predicting particle lift-off in different particle-fluid systems. The particulate flow conditions needed for lift-off is presented as the modified critical particle Reynolds number, $\check{\mathrm{Re}}^*_{\mathrm{p},d_V}$, which provided normalization for different channel hydraulic diameters, as a function of the modified Archimedes number, $\mathrm{Ar}^*_{d_V}$, which accounted for the effect of friction between the particle and channel wall. Deviation of the data for a single flat-plate particle from the generalized lift-off model was attributed to the effects of the electrostatic forces, particle trap inlet, and channel-particle domain size on the particle lift-off.

Although the CFD studies numerically resolved only the hydrodynamic forces on the particle, the electrostatic adhesion force was determined using the balance of the vertical forces, which include gravity, electrostatic, buoyant, and lift, acting on the particle positioned beyond L_e. The electrostatic adhesion force was determined to be 1.2×10^{-7} N, 2.0×10^{-7} N, and 1.3×10^{-7} N in isopropyl alcohol, water, and methanol, respectively. The electrostatic adhesion force was determined to be significant as it accounted for approximately 13 to 21% of the total downward vertical force. Since electrostatics played a significant factor in affecting the observed particle lift-off, it must be considered in both analysis of the lift-off data and development of a predictive model for lift-off.

5.4. Comparison of flat-plate lift-off data to generalized model

Fig. 10 maps the current data on flat-plate particle lift-off to a generalized model for lift-off (Rabinovich and Kalman, 2009a) of various particulate flow systems based on a power law relationship between the modified critical particle Reynolds number, $\check{\mathrm{Re}}^*_{\mathrm{p},d_V}$ (Eq. (7)), and the modified Archimedes number, $\mathrm{Ar}^*_{d_V}$ (Eq. (8)). Although the flat-plate particle lift-off data was generally comparable to that predicted using the generalized model, notable deviations may be observed. First, every range of values of the observed $\check{\mathrm{Re}}^*_{\mathrm{p},d_V}$ for a single flat-particle was significantly lower than the predicted $\check{\mathrm{Re}}^*_{\mathrm{p},d_V}$ from the generalized model at each $\mathrm{Ar}^*_{d_V}$ investigated. The reduction in the observed $\check{\mathrm{Re}}^*_{\mathrm{p},d_V}$ compared to that predicted using the generalized model may be attributed to the enhanced lift and drag forces acting on the flat-plate particle at the entrance of the current particulate flow system. Second, our results revealed the significant contribution of the channel-particle size to the particle lift-off. Specifically, the adjustment of HW/d_V^2 from 1.6 to 5.3 resulted in changes in $\check{\mathrm{Re}}^*_{\mathrm{p},d_V}$ by a factor of approximately 2 to 3. The large spread in $\check{\mathrm{Re}}^*_{\mathrm{p},d_V}$ at various HW/d_V^2 indicated wall-effects have a tremendous effect on particle lift-off behavior, even more notably for microchannel particulate flow systems such as the one used in the present study, in which the ratio of the particle diameter to channel diameter, d_V/D_H, ranges from 0.2 to 0.4 compared to 8×10^{-3} to 2×10^{-4} for relatively large particulate flow systems considered by Rabinovich and Kalman (2009a). Third, the observed $\check{\mathrm{Re}}^*_{\mathrm{p},d_V}$ as a function of $\mathrm{Ar}^*_{d_V}$ at each HW/d_V^2 deviated from the linear power law relationship of the generalized model. While Rabinovich and Kalman (2009a) used antistatic spray on the active channel surfaces to preclude electrostatic effects, the current experimental work considered electrostatic effects and revealed electrostatic adhesion forces to be significant. The magnitude of electrostatic forces on particles have been shown to be sensitive to the relative permittivity, ϵ_r, of the solvent in which the particles are immersed in, with lower ϵ_r resulting in stronger electrostatic coupling (Stojimirović et al., 2020). The magnitudes of the differing electrostatic adhesion forces acting on the particle resolved in Section 5.3 are reflective of the different ϵ_r of the solvents (Table 1) and extent of electrostatic shielding. As a result, ϵ_r of the solvent must also be accounted for in particulate lift-off studies in which electrostatic effects are significant.

5.5. Hydrodynamic forces on a flat-plate and spherical particle

From Figs. 5 and 10, the results from the single flat-plate particle flow experiments show that the observed shear Reynolds number and the modified particle Reynolds number, at each considered channel geometry, were lower than that predicted from models for spherical particles in previous works by Patankar et al. (2001) and Rabinovich and Kalman (2009a). Our experiments involve positioning the flat-plate particle in an entrance region with a constant circular cross-section, with three throughholes for fluidic inlets, lofted to the rectangular cross-section of varying channel dimensions. Conversely, Patankar et al. (2001) and Rabinovich and Kalman (2009a) position their particle away from the entrance. In our experiments, the flat-plate particle is positioned near one of the three throughholes, so it is expected that the particle experiences forces from the local fluid jet through the throughhole. Considering fluid flow continuity and an average fluid

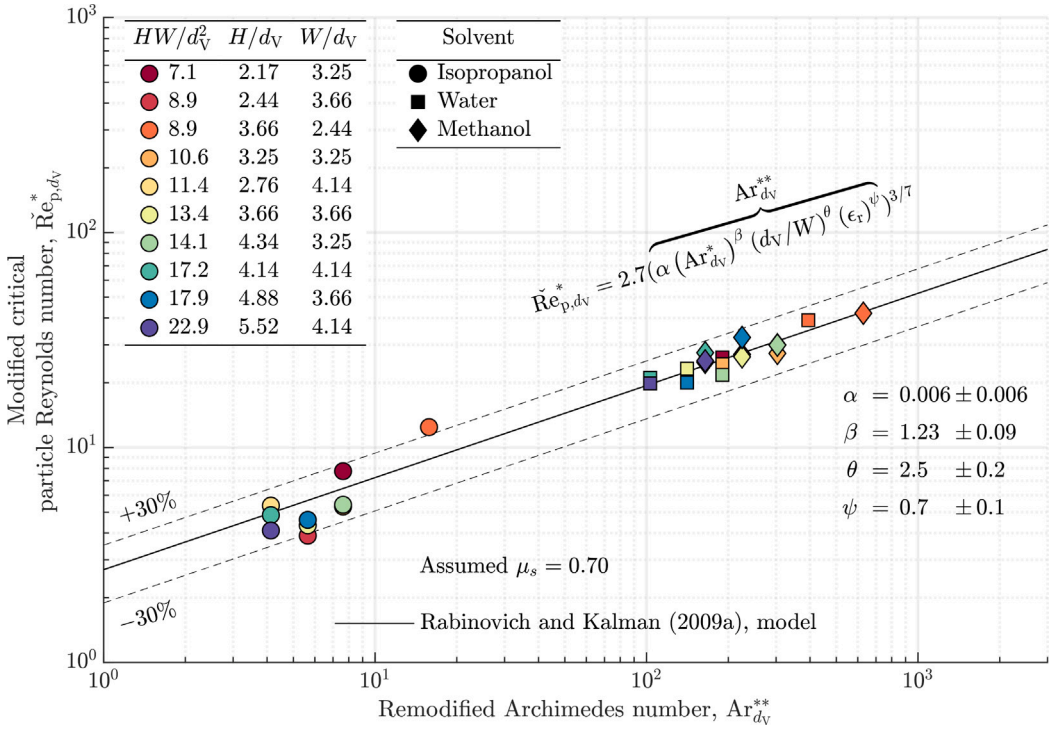

Fig. 11. Experimental data for single flat-particle lift-off mapped onto a corrected generalized curve, adapted from a generalized particle lift-off model from Rabinovich and Kalman (2009a), using a remodified Archimedes number, $\mathrm{Ar}^{**}_{d_V}$, to account for the effects of the channel-particle domain size, relative permittivity of the solvent, and the particle trap inlet on the particle lift-off. Empirical parameters, α, β, θ, and ψ, for the current particulate flow system were evaluated from a nonlinear regression model. The corrected single flat-plate particle data using $\mathrm{Ar}^{**}_{d_V}$ is in good agreement with the generalized curve for prediction of particle lift-off in terms of the modified critical particle Reynolds number, $\check{\mathrm{Re}}^*_{\mathrm{p},d_V}$.

velocity through the upstream main cylindrical channel, $\langle U_{\mathrm{main}}\rangle$, the average fluid velocity through one of the holes may be approximated as $\langle U_{\mathrm{hole}}\rangle = 2.1\langle U_{\mathrm{main}}\rangle$. Comparatively, the average fluid velocity through the considered rectangular channels ranges from $0.8\langle U_{\mathrm{main}}\rangle$ to $2.0\langle U_{\mathrm{main}}\rangle$. So, it is expected that the observed particle Reynolds number deviates from that predicted using the other models.

While the particle trap provides an enhancement in the lift and drag force, shown in Figs. 8 and 9, that may result in a lower observed particle Reynolds numbers needed for lift-off compared to predicted values, the deviation in the critical particle Reynolds numbers, as well as the observed particle-channel size dependency for lift-off, may also be explained by the arising hydrodynamic forces depending on the particle shape. At moderate particle Reynolds numbers ($1 \le \mathrm{Re}_{\mathrm{p}} \le 100$), the drag force on a spherical particle scales approximately to $F_{\mathrm{D,sphere}} \sim 1/2\,\rho\,\bar{u}_{\mathrm{p}}^2\,\pi\,(d/2)^2\,C_{\mathrm{D,sphere}}$ where $\bar{u}_{\mathrm{p}} = U - u_{\mathrm{p}}$ is the particle velocity relative to the local, superficial fluid velocity and where the drag force coefficient, $C_{\mathrm{D,sphere}}$, may be approximated using the Schiller–Naumann correlation (Schiller and Naumann, 1933). Similarly, the drag force on a flat-plate particle scales approximately to $F_{\mathrm{D,plate}} \sim 1/2\,\rho\,\bar{u}_{\mathrm{p}}^2\,w^2\,C_{\mathrm{D,plate}}$ where the drag coefficient, $C_{\mathrm{D,plate}}$, increases with larger angle of incidence and may be determined using direct numerical simulations (Zastawny et al., 2012; Sanjeevi et al., 2018). In our experiments, the angles of incidence for the flat-plate particle, initially positioned on top of the lofted region of the channel, varies depending on the channel configuration. Therefore, the particle-channel dimensions changes the resulting drag force acting on the flat-plate particle. For a spherical particle at moderate Re_{p}, the total lift force, composed of the shear-gradient and wall-induced lift contributions, scales as $F_{\mathrm{L,sphere}} \sim 1/2\,\rho\,\bar{u}_{\mathrm{p}}^2\,\pi\,(d/2)^2\,C_{\mathrm{L,sphere}}$ where the lift coefficient for a spherical particle is on the order of $C_{\mathrm{L,sphere}} \approx \mathcal{O}(10^{-1})$ (Cherukat and Mclaughlin, 1994; Bearman and Zdravkovich, 1978). For a flat-plate particle at moderate Re_{p} where the channel height is significantly greater than the lubrication gap ($H \gg \delta$), the total lift force acting on a flat-plate particle scales as $F_{\mathrm{L,plate}} \sim 1/2\,\rho\,\bar{u}_{\mathrm{p}}^2\,w^2\,C_{\mathrm{L,plate}}$, the lift force coefficient for a flat-plate particle is approximately $C_{\mathrm{L,plate}} \approx 6/(\mathrm{Re}_{\mathrm{p}}\,(\delta/w)^2)$ (Hamrock et al., 2004). For small gap sizes, the lift force coefficient on a flat-plate particle may grow to $C_{\mathrm{L,plate}} \approx \mathcal{O}(10^1 - 10^2)$. For a flat-plate particle sedimented flush with the bottom channel, this enhancement in lift requires the gap to first develop as a result of surface roughness or pressure lift on the corner chamfer of the particle. In our experiments, since the flat-plate particle sits in a lofted region near the particle trap, an immediate gap is present under the flat-plate particle that provides high pressure over the bottom particle surface and an enhancement in lift. A spherical particle, with its curved geometry and lack of a uniform lubrication pocket, would not benefit from this lift enhancement.

5.6. Correction to generalized lift-off model

A revision to the generalized lift-off model, with additional considerations of the effect of electrostatic, channel-particle size, and intrinsic properties of the particulate flow system, may be performed to predict the lift-off of a flat-plate particle in rectangular microchannel flows. As an initial model for prediction of lift-off of a flat-plate particle in rectangular microfluidic channels, a relationship between the critical particle Reynolds number and Archimedes number, similar to that from Rabinovich and Kalman (2009a), is proposed:

$$\check{\mathrm{Re}}^*_{\mathrm{p},d_V} = 2.7\mathrm{Ar}^{**\,3/7}_{d_V} \tag{25}$$

However, a remodified Archimedes number, $\mathrm{Ar}^{**}_{d_V}$, is introduced to account for the effects of $\mathrm{Ar}^*_{d_V}$, H/W, d_V/W, and ϵ_r with their respective empirical parameters, β, ξ, θ, ψ, and an additional α empirical modifier (Eq. (26)):

$$\mathrm{Ar}^{**}_{d_V} = \alpha\left(\mathrm{Ar}^*_{d_V}\right)^{\beta}(H/W)^{\xi}\left(d_V/W\right)^{\theta}\left(\epsilon_r\right)^{\psi} \tag{26}$$

Nonlinear regression of the parameters was performed using a Levenberg–Marquardt least squares method (Levenberg, 1944; Marquardt, 1963). Although the effect of H, more specifically $HW/d_{\max}^2$ and H/W, on lift-off was shown to be locally significant at each investigated Archimedes number, the results of the nonlinear regression yielded $\xi \approx 1$, indicating that H/W was not necessary for prediction of $\check{\mathrm{Re}}^*_{\mathrm{p},d_\mathrm{V}}$ over a large range of $\mathrm{Ar}^{**}_{d_\mathrm{V}}$. Thus, a simplified correction to the Archimedes number is proposed (Eq. (27)):

$$\mathrm{Ar}^{**}_{d_\mathrm{V}} = \alpha \left(\mathrm{Ar}^{*}_{d_\mathrm{V}}\right)^{\beta} \left(d_\mathrm{V}/W\right)^{\theta} \left(\epsilon_\mathrm{r}\right)^{\Psi} \tag{27}$$

Fig. 11 shows the comparison of the current lift-off data for a flat-plate particle to the corrected generalized lift-off model based on the relationship between the modified critical particle Reynolds number, $\check{\mathrm{Re}}^*_{\mathrm{p},d_\mathrm{V}}$, and the remodified Archimedes number, $\mathrm{Ar}^{**}_{d_\mathrm{V}}$. The lift-off data fits well with the revised lift-off model for a flat-plate particle with a root mean square error of 2.2 and largely remains within ± 30% of the model function. Despite the complexities of the particulate flow system due to the entrance and electrostatic effects, the revised lift-off model provides a simple model to predict the lift-off of the flat-plate particle.

The corrected generalized lift-off model proposed (Eq. (25)) offers a simple correction to the Archimedes number (Eq. (27)) to predict the critical particle Reynolds number necessary for lift-off of a single flat-plate particle in straight rectangular microchannels. The empirical modifiers for $\mathrm{Ar}^{*}_{d_\mathrm{V}}$, d_V/W, and ϵ_r, which may be easily evaluated using nonlinear regression, accounts for the entrance, channel geometry, and electrostatic effects of the particular particulate flow system of interest.

While our analysis examines the effects of HW/d^2, H/d, and W/d on the critical lift-off, it is acknowledged that since the particulate flow experiments consisted of only a single type of particle, our findings reflect only the effect of the channel dimensions on lift-off. Further studies with different particle sizes and channel dimensions, as well as a larger range of particle-channel size ratios, would be needed for validation of the model. Also, for pragmatic applications, our particulate flow experiments were performed with the flat-plate particle initially positioned in a specialized entrance region with a particle trap. Additional studies may be performed with the particle positioned away from the entrance region. In addition, our work considers only three solvents and for the particular microchip particle used, a range of Archimedes numbers, $\mathrm{Ar}_{d_\mathrm{V}}$, from 191 to 2820. The range of $\mathrm{Ar}_{d_\mathrm{V}}$ covered in our work provides a good basis for generalizable predictability of the critical lift-off of a flat-plate particle since it encompasses 50% of 42 common solvents, ranging in kinematic viscosity from 3.3×10^{-7} to 3.7×10^{-6} m^2/s, used for organic synthesis and high-performance liquid chromatography (Przybytek, 1980). Further validation studies with additional solvents are needed to ensure the model may be extended to a larger range of particulate flow configurations.

6. Conclusions

The critical lift-off of a single flat-plate microchip particle in straight, horizontal, rectangular microchannels was investigated using both experimental characterization and numerical simulation studies. The channel-particle domain size, HW/d^2, and the channel aspect ratio, H/W, were determined to affect lift-off, as lower $\check{\mathrm{Re}}_{\mathrm{s},d_{\max}}$ was observed for higher HW/d^2 at each $\mathrm{Ar}_{d_{\max}}$ considered. From numerical particulate flow simulations, electrostatic adhesion forces acting on the particle were determined to be significant. Based on the experimental particulate flow studies, the critical particle Reynolds number as a function of a corrected Archimedes number, which accounted for the channel width, particle diameter, solvent relative permittivity, and intrinsic properties of the particulate flow system, was found to provide an excellent empirical correlation to predict the lift-off of a single flat-plate particle. The developed empirical model for lift-off of a single microchip provides an accurate, first model for predicting the lift-off of a flat-plate particle under different microchannel and solvent configurations while accounting for entrance, wall, and electrostatic effects. The work provides a connection and knowledge transfer between the fields of pneumatic/hydraulic conveying and microfluidics towards furthering the understanding of particulate flow dynamics.

Nomenclature

Symbols

a	Empirical parameter, Eq. (5)
A	Channel cross-sectional area = HW (m^2)
AR	Channel aspect ratio = H/W (m)
Ar_d	Archimedes number based on the characteristic particle diameter = $\rho_\mathrm{f}(\rho_\mathrm{p} - \rho_\mathrm{f})gd^3/\mu^2$ (–)
$\mathrm{Ar}_{d_{\max}}$	Archimedes number based on particle rotational diameter = $\rho_\mathrm{f}(\rho_\mathrm{p} - \rho_\mathrm{f})gd_{\max}^3/\mu^2$ (–)
$\mathrm{Ar}_{d_\mathrm{V}}$	Archimedes number based on equivalent volume spherical particle diameter = $\rho_\mathrm{f}(\rho_\mathrm{p} - \rho_\mathrm{f})gd_\mathrm{V}^3/\mu^2$ (–)
$\mathrm{Ar}^*_{d_\mathrm{V}}$	Modified Archimedes number based on equivalent volume spherical particle diameter = $\mathrm{Ar}_{d_\mathrm{V}}\mu_\mathrm{s}$ (–)
b	Empirical parameter, Eq. (5)
c	Empirical parameter, Eq. (6)
C_D	Drag force coefficient (–)
C_L	Lift force coefficient (–)
d	Characteristic particle diameter (m)
D	Channel diameter (m)
D_{50}	Reference 50 mm channel diameter (m)
D_H	Channel hydraulic diameter (m)
$d_{\max}$	Particle rotational diameter (m)
d_V	Equivalent volume spherical particle diameter (m)
$e_{\mathrm{nb,max}}$	Boundary maximum element size (m)
$e_{\mathrm{nb,min}}$	Boundary minimum element size (m)
$e_{\mathrm{ng,max}}$	Global maximum element size (m)
$e_{\mathrm{ng,min}}$	Global minimum element size (m)
$\mathbf{F}_\mathrm{A}$	Adhesion force (N)
$\mathbf{F}_\mathrm{B}$	Buoyant force = $\rho_\mathrm{f}V_\mathrm{f}g$ (N)
$\mathbf{F}_\mathrm{D}$	Drag force (N)
$\mathbf{F}_\mathrm{F}$	Friction force (N)
$\mathbf{F}_\mathrm{G}$	Gravity force = $-\rho_\mathrm{p}V_\mathrm{p}g$ (N)
$\mathbf{F}_\mathrm{L}$	Lift force (N)
Fr_d	Froude number based on characteristic particle diameter = $\langle U\rangle/\sqrt{gd}$ (–)
g	Standard acceleration of gravity (m/s^2)
$\mathbf{g}$	Gravitational field (m/s^2)
h	Particle height (m)
H	Channel height (m)
$\mathbf{I}$	Identity matrix (–)
k	Function of specific properties affecting the specific threshold suspension that adjusts the modified Archimedes number based on equivalent volume spherical particle diameter, Eq. (6)
L	Channel length (m)
L_e	Entrance length for rectangular channel = $0.058D_\mathrm{H}\mathrm{Re}$ (m)
ΔL_p	Axial distance of particle from inlet (m)
m	Empirical power term, Eq. (6)
$\mathbf{n}_x$	Outward unit normal vector in x-direction (–)

$\mathbf{n}_y$	Outward unit normal vector in y-direction (–)
p	Pressure (Pa)
Q	Volumetric fluid flow rate (m^3/s)
$\check{Q}$	Critical volumetric fluid flow rate for lift-off (m^3/s)
r	Function of pipe diameter that adjusts the critical particle Reynolds number based on equivalent volume spherical particle diameter, Eq. (6)
Re	Reynolds number = $\rho_f \langle U \rangle D_H/\mu$ (–)
$\mathrm{Re}_{p,d}$	Particle Reynolds number based on the characteristic particle diameter (–)
$\check{\mathrm{Re}}_{p,d_V}$	Critical particle Reynolds number based on equivalent volume spherical particle diameter = $(d_V/D_H)^2\mathrm{Re}$ (–)
$\check{\mathrm{Re}}^*_{p,d_V}$	Modified critical particle Reynolds number based on equivalent volume spherical particle diameter = $\mathrm{Re}_{p,d_V}/(1.25 - 0.5\exp((D_H/D_{50})/1.5))$ (–)
$\mathrm{Re}_{s,d}$	Shear Reynolds number based on the characteristic particle diameter (–)
$\check{\mathrm{Re}}_{s,d_{max}}$	Critical shear Reynolds number based on particle rotational diameter (–)
S	Particle surface (m^2)
$\mathbf{u}$	Fluid velocity vector (m/s)
U	Superficial fluid velocity (m/s)
U_*	Shear velocity (m/s)
$\langle U \rangle$	Average fluid velocity (m/s)
$\bar{u}_p$	Particle velocity relative to the local superficial fluid velocity (m/s)
U_{max}	Maximum fluid velocity (m/s)
V_f	Volume of displaced fluid (m^3)
V_p	Volume of particle (m^3)
w	Particle width (m)
W	Channel width (m)

Greek Symbols

α	Empirical multiplier for remodified Archimedes number, Eqs. (26) and (27)
β	Empirical power adjusting effect of modified Archimedes number, Eqs. (26) and (27)
δ	Vertical distance between particle and wall (m)
δ_c	Clearance distance between particle and wall (m)
ϵ_r	Relative permittivity or dielectric constant (–)
$\langle \dot{\gamma}_w \rangle$	Average shear rate at the bottom channel wall (s^{-1})
μ	Dynamic viscosity of fluid (Pa s)
μ_{kf}	Kinetic friction coefficient between particle and wall (–)
μ_{sf}	Static friction coefficient between particle and wall (–)
∇	Del operator (m^{-1})
ϕ	Particle sphericity, ratio of surface area of an equivalent volume sphere to the surface area of the particle (–)
ψ	Empirical power adjusting effect of ϵ_r, Eqs. (26) and (27)
ρ_f	Density of fluid (kg/m^3)
ρ_p	Density of particle (kg/m^3)
$\boldsymbol{\sigma}$	Total stress tensor (Pa)
τ	Shear stress (Pa)
$\boldsymbol{\tau}$	Viscous stress tensor (Pa)
θ	Empirical power adjusting effect of D/W, Eqs. (26) and (27)
ξ	Empirical power adjusting effect of H/W, Eq. (26)

Top Accents

ˇ	Critical

Subscripts

A	Adhesion
B	Buoyant
D	Drag
e	Entrance
f	Fluid
F	Friction
G	Gravity
H	Hydraulic
kf	Kinetic friction
L	Lift
max	Maximum
min	Minimum
nb	Numerical boundary
ng	Numerical global
p	Particle
r	Relative
sf	Static friction
s	Shear
w	Wall

Superscripts

*	Modified
T	Transpose

Abbreviations

ALE	Arbitrary Lagrangian–Eulerian
CCF	Central composite face-centered
CFD	Computational fluid dynamics
CNC	Computer numerical control
HC	Hydraulic conveying
PC	Pneumatic conveying
PMMA	Poly(methyl methacrylate)

CRediT authorship contribution statement

Raymond Yeung: Writing – review & editing, Writing – original draft, Visualization, Methodology, Investigation, Formal analysis, Data curation, Conceptualization. **Cynthia Sainz:** Investigation, Data curation. **Jason Mandala:** Software. **Philip Brisk:** Writing – review & editing, Writing – original draft, Supervision, Resources, Project administration, Funding acquisition. **William H. Grover:** Writing – review & editing, Writing – original draft, Supervision, Resources, Project administration, Methodology, Funding acquisition, Formal analysis. **Victor G.J. Rodgers:** Writing – review & editing, Writing – original draft, Supervision, Project administration, Methodology, Funding acquisition, Formal analysis, Conceptualization.

Declaration of competing interest

The authors declare the following financial interests/personal relationships which may be considered as potential competing interests: Victor G. J. Rodgers reports financial support was provided by National Science Foundation. Philip Brisk reports financial support was provided by National Science Foundation. William H. Grover reports financial support was provided by National Science Foundation. Raymond Yeung reports financial support was provided by National Science Foundation. Jason Mandala reports financial support was provided by National Science Foundation. Cynthia Sainz reports financial support was provided by University of California, Riverside. If there are other authors, they declare that they have no known competing financial interests or personal relationships that could have appeared to influence the work reported in this paper.

Acknowledgments

This material is based upon work supported by the National Science Foundation, United States under the Cyber–Physical Systems Award (Grant No. NSF-1740052), the Jacques S. Yeager, Sr. Professorship, and the University of California, Riverside Minigrant for Undergraduate Research and Creative Activities. We thank Richard Morris, Wlodek Mandecki, and Wesley Kopacka (p-Chip Corporation, Chicago, IL; formerly PharmaSeq, Inc., Monmouth Junction, NJ) for providing microtransponders and for their insightful discussions on microchip manipulation and sorting.

Appendix A. Supplementary data

Supplementary material related to this article can be found online at https://doi.org/10.1016/j.ijmultiphaseflow.2025.105355.

Data availability

Data will be made available on request.

References

Amini, H., Lee, W., Carlo, D.D., 2014. Inertial microfluidic physics. Lab Chip 14 (15), 2739–2761. http://dx.doi.org/10.1039/C4LC00128A.

Bearman, P.W., Zdravkovich, M.M., 1978. Flow around a circular cylinder near a plane boundary. J. Fluid Mech. 89 (1), 33–47. http://dx.doi.org/10.1017/S002211207800244X.

Bergman, T.L., 2011. Fundamentals of Heat and Mass Transfer. John Wiley & Sons.

Birtwell, S., Morgan, H., 2009. Microparticle encoding technologies for high-throughput multiplexed suspension assays. Integr. Biol. 1 (5–6), 345–362. http://dx.doi.org/10.1039/b905502a.

Buckingham, E., 1914. On physically similar systems; Illustrations of the use of dimensional equations. Phys. Rev. 4 (4), 345–376. http://dx.doi.org/10.1103/PhysRev.4.345.

Cabrejos, F.J., Klinzing, G.E., 1992. Incipient motion of solid particles in horizontal pneumatic conveying. Powder Technol. 72 (1), 51–61. http://dx.doi.org/10.1016/S0032-5910(92)85021-M.

Cabrejos, F.J., Klinzing, G.E., 1994. Pickup and saltation mechanisms of solid particles in horizontal pneumatic transport. Powder Technol. 79 (2), 173–186. http://dx.doi.org/10.1016/0032-5910(94)02815-X.

Cherukat, P., Mclaughlin, J.B., 1994. The inertial lift on a rigid sphere in a linear shear flow field near a flat wall. J. Fluid Mech. 263, 1–18. http://dx.doi.org/10.1017/S0022112094004015.

Cunin, F., Schmedake, T.A., Link, J.R., Li, Y.Y., Koh, J., Bhatia, S.N., Sailor, M.J., 2002. Biomolecular screening with encoded porous-silicon photonic crystals. Nat. Mater. 1 (1), 39–41. http://dx.doi.org/10.1038/nmat702.

Eun Chung, S., Ah Lee, S., Kim, J., Kwon, S., 2009. Optofluidic encapsulation and manipulation of silicon microchips using image processing based optofluidic maskless lithography and railed microfluidics. Lab Chip 9 (19), 2845–2850. http://dx.doi.org/10.1039/B903760H.

Gallily, I., Cohen, A.-H., 1979. On the orderly nature of the motion of nonspherical aerosol particles. II. Inertial collision between a spherical large droplet and an axially symmetrical elongated particle. J. Colloid Interface Sci. 68 (2), 338–356. http://dx.doi.org/10.1016/0021-9797(79)90287-X.

Gibbings, J.C., 2011. Dimensional Analysis. Springer Science & Business Media.

Gruda, M.C., Pinto, A., Craelius, A., Davidowitz, H., Kopacka, W.M., Li, J., Qian, J., Rodriguez, E., Kuspiel, E., Mandecki, W., 2010. A system for implanting laboratory mice with Light-Activated microtransponders. J. Am. Assoc. Lab. Anim. Sci. 49 (6), 826–831.

Halow, J.S., 1973. Incipient rolling, sliding and suspension of particles in horizontal and inclined turbulent flow. Chem. Eng. Sci. 28 (1), 1–12. http://dx.doi.org/10.1016/0009-2509(73)85080-8.

Hamrock, B.J., Schmid, S.R., Jacobson, B.O., 2004. Fundamentals of Fluid Film Lubrication, second ed. CRC Press.

Han, Q., Hunt, J.D., 1995. Particle pushing: Critical flow rate required to put particles into motion. J. Cryst. Growth 152 (3), 221–227. http://dx.doi.org/10.1016/0022-0248(95)00085-2.

Hoffmann, D., Brennan, D., Loughran, M., 2006. Injection and manipulation of silicon microbeads in a customized microfluidic platform. In: Microfluidics, BioMEMS, and Medical Microsystems IV. Vol. 6112, SPIE, pp. 103–110. http://dx.doi.org/10.1117/12.660342.

Hoffmann, D., Curtin, M., Loughran, M., 2007a. An integrated microsystem for multiplex processing of encoded silicon microbeads. In: Microfluidics, BioMEMS, and Medical Microsystems V. Vol. 6465, SPIE, pp. 109–116. http://dx.doi.org/10.1117/12.702565.

Hoffmann, D., O'Brien, J., Brennan, D., Loughran, M., 2007b. Optically encoded silicon microbeads: Detection and characterisation in a microfluidic system. Sensors Actuators B: Chem. 122 (2), 653–658. http://dx.doi.org/10.1016/j.snb.2006.07.023.

Hubbe, M.A., 1984. Theory of detachment of colloidal particles from flat surfaces exposed to flow. Colloids Surf. 12, 151–178. http://dx.doi.org/10.1016/0166-6622(84)80096-7.

Hubert, M., Kalman, H., 2004. Measurements and comparison of saltation and pickup velocities in wind tunnel. Granul. Matter 6 (2), 159–165. http://dx.doi.org/10.1007/s10035-004-0166-x.

Hur, S.C., Choi, S.-E., Kwon, S., Carlo, D.D., 2011. Inertial focusing of non-spherical microparticles. Appl. Phys. Lett. 99 (4), 044101. http://dx.doi.org/10.1063/1.3608115.

Jensen-McMullin, C., Bachman, M., Li, G.P., 2008. Microfabricated micropallets for enhancement of biomolecular techniques. Microfluid. Nanofluidics 5 (2), 225–234. http://dx.doi.org/10.1007/s10404-007-0240-x.

Kalman, H., 2022. Role of Reynolds and archimedes numbers in particle-fluid flows. Rev. Chem. Eng. 38 (2), 149–165. http://dx.doi.org/10.1515/revce-2020-0005.

Kalman, H., Satran, A., Meir, D., Rabinovich, E., 2005. Pickup (critical) velocity of particles. Powder Technol. 160 (2), 103–113. http://dx.doi.org/10.1016/j.powtec.2005.08.009.

Karam, M., Saad, T., 2021. BuckinghamPy: A Python software for dimensional analysis. SoftwareX 16, 100851. http://dx.doi.org/10.1016/j.softx.2021.100851.

Krishnan, G.P., Leighton Jr., D.T., 1995. Inertial lift on a moving sphere in contact with a plane wall in a shear flow. Phys. Fluids 7 (11), 2538–2545. http://dx.doi.org/10.1063/1.868755.

Lee, H., Balachandar, S., 2017. Effects of wall roughness on drag and lift forces of a particle at finite Reynolds number. Int. J. Multiph. Flow 88, 116–132. http://dx.doi.org/10.1016/j.ijmultiphaseflow.2016.09.006.

Leighton, D., Acrivos, A., 1985. The lift on a small sphere touching a plane in the presence of a simple shear flow. Z. Angew. Math. Phys. ZAMP 36 (1), 174–178. http://dx.doi.org/10.1007/BF00949042.

Levenberg, K., 1944. A method for the solution of certain non-linear problems in least squares. Quart. Appl. Math. 2 (2), 164–168. http://dx.doi.org/10.1090/qam/10666.

Li, J., Veltri, R.W., Yuan, Z., Christudass, C.S., Mandecki, W., 2015. Macrophage inhibitory cytokine 1 biomarker serum immunoassay in combination with PSA is a more specific diagnostic tool for detection of prostate cancer. PLoS One 10 (4), e0122249. http://dx.doi.org/10.1371/journal.pone.0122249.

Li, J., Wang, Z., Gryczynski, I., Mandecki, W., 2010. Silver nanoparticle-enhanced fluorescence in microtransponder-based immuno- and dnahybridization assays. Anal. Bioanal. Chem. 398 (5), 1993–2001. http://dx.doi.org/10.1007/s00216-010-4108-7.

Liga, A., Morton, J.A.S., Kersaudy-Kerhoas, M., 2016. Safe and Cost-Effective Rapid-Prototyping of multilayer PMMA microfluidic devices. Microfluid. Nanofluidics 20 (12), 164. http://dx.doi.org/10.1007/s10404-016-1823-1.

Lin, X., Flint, J.A., Azaro, M., Coradetti, T., Kopacka, W.M., Streck, D.L., Wang, Z., Dermody, J., Mandecki, W., 2007. Microtransponder-Based Multiplex Assay for genotyping cystic fibrosis. Clin. Chem. 53 (7), 1372–1376. http://dx.doi.org/10.1373/clinchem.2006.081810.

Mandecki, W., Ardelt, B., Coradetti, T., Davidowitz, H., A. Flint, J., Huang, Z., M. Kopacka, W., Lin, X., Wang, Z., Darzynkiewicz, Z., 2006. Microtransponders, the miniature RFID electronic chips, as platforms for cell growth in cytotoxicity assays. Cytom. A 69A (11), 1097–1105. http://dx.doi.org/10.1002/cyto.a.20344.

Mandø, M., Rosendahl, L., 2010. On the motion of non-spherical particles at high Reynolds number. Powder Technol. 202 (1), 1–13. http://dx.doi.org/10.1016/j.powtec.2010.05.001.

Marquardt, D.W., 1963. An algorithm for least-squares estimation of nonlinear parameters. J. Soc. Ind. Appl. Math. 11 (2), 431–441. http://dx.doi.org/10.1137/0111030.

Martinez, R.C., Sweeney, L.G., Finlay, W.H., 2009. Aerodynamic forces and moment on a sphere or cylinder attached to a wall in a blasius boundary layer. Eng. Appl. Comput. Fluid Mech. 3 (3), 289–295. http://dx.doi.org/10.1080/19942060.2009.11015272.

Palakurthi, N.K., Ghia, U., Turkevich, L., 2017. Simulations of particle detachment from a flat surface. In: ASME 2017 Fluids Engineering Division Summer Meeting. American Society of Mechanical Engineers Digital Collection, http://dx.doi.org/10.1115/FEDSM2017-69111.

Patankar, N.A., Huang, P.Y., Ko, T., Joseph, D.D., 2001. Lift-off of a single particle in Newtonian and viscoelastic fluids by direct numerical simulation. J. Fluid Mech. 438, 67–100. http://dx.doi.org/10.1017/S0022112001004104.

Przybytek, J.T., 1980. High-Purity Solvent Guide, vol. 53, Burdick and Jackson Laboratories.

Rabinovich, E., Kalman, H., 2007. Pickup, critical and wind threshold velocities of particles. Powder Technol. 176 (1), 9–17. http://dx.doi.org/10.1016/j.powtec.2007.01.033.

Rabinovich, E., Kalman, H., 2008. Generalized master curve for threshold superficial velocities in Particle–Fluid systems. Powder Technol. 183 (2), 304–313. http://dx.doi.org/10.1016/j.powtec.2007.07.030.

Rabinovich, E., Kalman, H., 2009a. Incipient motion of individual particles in horizontal Particle–Fluid systems: A. Experimental analysis. Powder Technol. 192 (3), 318–325. http://dx.doi.org/10.1016/j.powtec.2009.01.013.

Rabinovich, E., Kalman, H., 2009b. Incipient motion of individual particles in horizontal Particle–Fluid systems: B. Theoretical analysis. Powder Technol. 192 (3), 326–338. http://dx.doi.org/10.1016/j.powtec.2009.01.014.

Rich, R., Li, J., Fudala, R., Gryczynski, Z., Gryczynski, I., Mandecki, W., 2012. Properties of coatings on RFID P-Chips that support plasmonic fluorescence enhancement in bioassays. Anal. Bioanal. Chem. 404 (8), 2223–2231. http://dx.doi.org/10.1007/s00216-012-6369-9.

Sanjeevi, S.K.P., Kuipers, J.A.M., Padding, J.T., 2018. Drag, lift and torque correlations for non-spherical particles from Stokes limit to high Reynolds numbers. Int. J. Multiph. Flow 106, 325–337. http://dx.doi.org/10.1016/j.ijmultiphaseflow.2018.05.011.

Schiller, L., Naumann, A., 1933. A drag coefficient correlation. Zeit. Ver. Dtsch. Ing. 77, 318–320.

Sharma, M.M., Chamoun, H., Sarma, D.S.H.S.R., Schechter, R.S., 1992. Factors controlling the hydrodynamic detachment of particles from surfaces. J. Colloid Interface Sci. 149 (1), 121–134. http://dx.doi.org/10.1016/0021-9797(92)90398-6.

Shukla, N., Henthorn, K.H., 2009. Effect of relative particle size on large particle detachment from a microchannel. Microfluid. Nanofluidics 6 (4), 521–527. http://dx.doi.org/10.1007/s10404-008-0330-4.

Slocum, A., 2010. Kinematic couplings: A review of design principles and applications. Int. J. Mach. Tools Manuf. 50 (4), 310–327. http://dx.doi.org/10.1016/j.ijmachtools.2009.10.006.

Stevenson, P., Thorpe, R.B., Davidson, J.F., 2002. Incipient motion of a small particle in the viscous boundary layer at a pipe wall. Chem. Eng. Sci. 57 (21), 4505–4520. http://dx.doi.org/10.1016/S0009-2509(02)00418-9.

Stojimirović, B., Galli, M., Trefalt, G., 2020. Forces between silica particles in isopropanol solutions of 1:1 electrolytes. Phys. Rev. Res. 2 (2), 023315. http://dx.doi.org/10.1103/PhysRevResearch.2.023315.

Truskey, G.A., Yuan, F., Katz, D.F., 2004. Transport Phenomena in Biological Systems. Pearson/Prentice Hall Upper Saddle River, NJ, USA:.

Vastl, J., Wang, T., Trinh, T.B., Spiegel, D.A., 2017. Encoded Silicon-Chip-Based Platform for combinatorial synthesis and screening. ACS Comb. Sci. 19 (4), 255–261. http://dx.doi.org/10.1021/acscombsci.6b00181.

Xiao, X.-Y., Li, R., Zhuang, H., Ewing, B., Karunaratne, K., Lillig, J., Brown, R., Nicolaou, K., 2000. Solid-phase combinatorial synthesis using MicroKan reactors, Rf tagging, and directed sorting. Biotechnol. Bioeng. 71 (1), 44–50. http://dx.doi.org/10.1002/(SICI)1097-0290(200024)71:1<44::AID-BIT7>3.0.CO;2-J.

Zastawny, M., Mallouppas, G., Zhao, F., van Wachem, B., 2012. Derivation of drag and lift force and torque coefficients for non-spherical particles in flows. Int. J. Multiph. Flow 39, 227–239. http://dx.doi.org/10.1016/j.ijmultiphaseflow.2011.09.004.

Zeng, L., Najjar, F., Balachandar, S., Fischer, P., 2009. Forces on a finite-sized particle located close to a wall in a linear shear flow. Phys. Fluids 21 (3), http://dx.doi.org/10.1063/1.3082232.